CARRIER RECOVERY IN BURST-MODE 16-QAM

A Thesis Submitted to the College of

Graduate Studies and Research

in Partial Fulfillment of the Requirements

for the Degree of Master of Science

in the Department of Electrical Engineering

University of Saskatchewan

Saskatoon, Saskatchewan

by

Jingxin Chen

June 2004

PERMISSION TO USE

In presenting this thesis in partial fulfillment of the requirements for a Postgraduate degree from the University of Saskatchewan, the author agrees that the Libraries of this University may make it freely available for inspection. The author further agree that permission for copying of this thesis in any manner, in whole or in part, for scholarly purposes may be granted by the professor who supervised this thesis work or, in his absence, by the Head of the Department or the Dean of the College of Graduate Studies and Research at the University of Saskatchewan. It is understood that any copying or publication or use of this thesis or parts thereof for financial gain shall not be allowed without the author's written permission. It is also understood that due recognition shall be given to me and to the University of Saskatchewan in any scholarly use which may be made of any material in my thesis.

Requests for permission to copy or to make other use of material in this thesis in whole or part should be addressed to:

Head of the Department of Electrical Engineering
University of Saskatchewan
Saskatoon, Saskatchewan, Canada
S7N 5A9

ABSTRACT

Wireless communication systems such as multipoint communication systems (MCS) are becoming attractive as cost-effective means for providing network access in sparsely populated, rugged, or developing areas of the world. Since the radio spectrum is limited, it is desirable to use spectrally efficient modulation methods such as quadrature amplitude modulation (QAM) for high data rate channels. Many MCS employ time division multiple access (TDMA) and/or time division duplexing (TDD) techniques, in which transmissions operate in bursts. In many cases, a preamble of known symbols is appended to the beginning of each burst for carrier and symbol timing recovery (symbol timing is assumed known in this thesis). Preamble symbols consume bandwidth and power and are not used to convey information. In order for burst-mode communications to provide efficient data throughput, the synchronization time must be short compared to the user data portion of the burst.

Traditional methods of communication system synchronization such as phase-locked loops (PLLs) have demonstrated reduced performance when operated in burst-mode systems. In this thesis, a feedforward (FF) digital carrier recovery technique to achieve rapid carrier synchronization is proposed. The estimation algorithms for determining carrier offsets in carrier acquisition and tracking in a linear channel environment corrupted by additive white Gaussian noise (AWGN) are described. The estimation algorithms are derived based on the theory of maximum likelihood (ML) parameter estimation. The estimations include data-aided (DA) carrier frequency and phase estimations in acquisition and non-data-aided (NDA) carrier phase estimation in tracking. The DA carrier frequency and phase estimation algorithms are based on oversampling of a known preamble. The NDA carrier phase estimation makes use of symbol timing knowledge and estimates are extracted from the random data portion of the burst. The algorithms have been simulated and tested using Matlab® to verify their

functionalities. The performance of these estimators is also evaluated in the burst-mode operations for 16-QAM and compared in the presence of non-ideal conditions (frequency offset, phase offset, and AWGN). The simulation results show that the carrier recovery techniques presented in this thesis proved to be applicable to the modulation schemes of 16-QAM. The simulations demonstrate that the techniques provide a fast carrier acquisition using a short preamble (about 111 symbols) and are suitable for burst-mode communication systems.

ACKNOWLEDGEMENTS

I would like to express my sincere gratitude to my supervisor, Professor David M. Klymyshyn, for being the guiding force behind the research necessary for the completion of this thesis. Without his guidance, encouragement, support, ideas, and scientific enlightenment this work would not have been possible.

I also extend my sincere gratitude to Professor Ha Nguyen who performed as my acting supervisor in the final stage of this work, when Professor Klymyshyn was away and worked on research in Germany. Professor Nguyen has been abundantly helpful and given me a lot of valuable advice on my final oral exam and thesis.

My great appreciation also goes to the management and staff of TRLabs in Saskatoon for providing support and wonderful research environment. My thanks especially go to Jack Hanson, Dan Aspel, Trevor Hamm, and Garth Wells who always provided me technical help as I needed.

Finally, I would like to thank my parents, Shang Xun Chen and Yi Wen Rong, my parents-in-law, my husband Peter, and my friends for all the encouragement and support they have provided me throughout my academic career. No words can express my gratitude to them.

DEDICATION

To my adorable daughter, *Yuan Yuan*

TABLE OF CONTENTS

LIST OF FIGURES

LIST OF TABLES

LIST OF ABBREVIATIONS

ASK	Amplitude Shift Keying
AWGN	Additive White Gaussian Noise
BER	Bit Error Rate
bps	Bit Per Second
DA	Data-Aided
dB	Decibels
DD	Decision Directed
DQPSK	Differential Quadrature Phase Shift Keying
DSL	Digital Subscriber Line
DSP	Digital Signal Processing
FB	FeedBack
FF	FeedForward
FSK	Frequency Shift Keying
I	Inphase
IF	Intermediate Frequency
ISI	InterSymbol Interference
LO	Local Oscillator
LOS	Line Of Sight
LPF	LowPass Filters
MAN	Metropolitan Area Networks

MAP	Maximum A Posteriori
MCS	Multipoint Communication Systems
ML	Maximum Likelihood
NDA	Non-Data-Aided
PAM	Pulse Amplitude Modulation
pdf	Probability Density Function
PLL	Phase-Locked Loop
ppm	Part Per Million
PSD	Power Spectral Density
PSK	Phase Shifting Keying
Q	Quadrature
QAM	Quadrature Amplitude Modulation
QPSK	Quadrature Phase Shift Keying
RC	Raised Cosine
RF	Radio Frequency
RMS	Root Mean Square
RRC	Root Raised Cosine
SNR	Signal-to-Noise Ratio
sps	Symbol Per Second
TDD	Time Division Duplexing
TDMA	Time Division Multiple Access
V&V	Viterbi and Viterbi

LIST OF SYMBOLS

A_m	Amplitude of the m^{th} symbol
B	Bandwidth
E_s	Symbol energy
E_b	Bit energy
E_b/N_0	Signal-to-noise ratio per bit
f_c	Carrier frequency
f_0	Local carrier frequency
f	Carrier frequency offset
$\hat{f}$	Carrier frequency offset estimate
Δf	Residual frequency error
$g(t)$	Pulse shaping signal
I_n	16-QAM symbols
K	The number of bits per symbol
k	Sampling index
L	Arbitrary positive integer
M	The size of the QAM constellation
n	Symbol index
N_0	Noise power spectral density

P_s	Probability of symbol error
P_b	Probability of bit error
R	Symbol rate
R_b	Bit rate
r	Roll-off factor
$r(t)$	Received signal
$s(t)$	Transmitted signal
S/N	Signal-to-noise ratio
T	Symbol duration
T_s	Sample duration
$u(t)$	Baseband equivalent signal
$v(t)$	AWGN noise
θ_m	Phase of the m^{th} symbol
Ω	Carrier frequency offset
$\hat{\Omega}$	Carrier frequency offset estimate
$\Delta\Omega$	Residual frequency error
ϕ_c	Carrier phase
ϕ_0	Local carrier phase
ϕ	Carrier phase offset
$\hat{\phi}$	Carrier phase offset estimate in acquisition
$\Delta\phi$	Phase estimation error

$\hat{\Phi}$	Phase estimate in tracking
$\delta(t)$	Impulse function
σ^2	Variance
Δ	Constant

Chapter 1

INTRODUCTION

1.1 Background

There is tremendous worldwide demand for high-speed connections to data networks. High-speed "wired" connections which are becoming common in developed areas, include optical fibre, coaxial cable, and digital subscriber line (DSL) over copper phone lines. Wired connections are often very expensive to deploy in areas not well supported by developed network infrastructure. Therefore, it is unlikely that high bandwidth "wired" data access methods will be widely available in sparsely populated, rugged, or developing areas of the world.

Wireless systems such as multipoint communication systems (MCS) are becoming attractive as a cost-effective means for providing network access in these situations. A simple wireless MCS system architecture is shown in Figure 1.1. This system has a "hub" terminal connected to the high-speed backbone network and communicates with a number of fixed remote terminals (users) in the wireless channel.

Many of these systems employ forms of "channel sharing" in time, using various time division multiple access (TDMA) and/or time division duplexing (TDD) techniques. TDMA is a method which enables users to access the assigned bandwidth for a fraction of the time, called a slot, on a periodic basis. TDD system uses a common frequency radio channel in both transmit (Tx) and receive (Rx) directions, and in particular results in an efficient use of the radio spectrum. Besides, these techniques can simplify radio hardware, accommodate variable user data rates, and support new services.

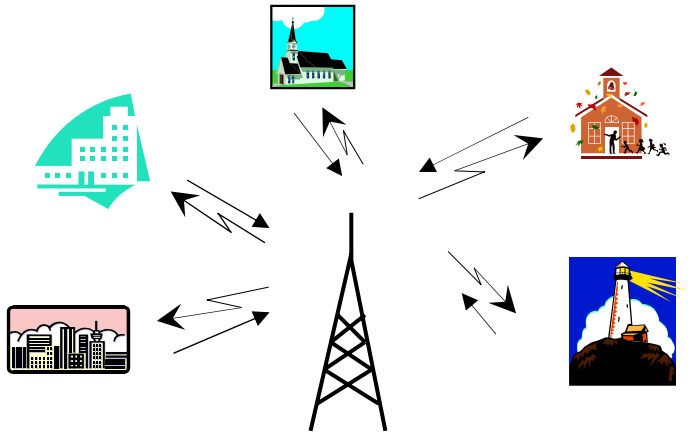

Figure 1.1 Architecture of a wireless MCS system

Due to transmission bandwidth restrictions and higher data rate demand, modulation schemes of higher order are needed to allow more "bits/s/Hz" to be transmitted. *M-ary quadrature amplitude modulation* (QAM) for $M \geq 16$ is a possible candidate to achieve higher spectral efficiency and narrow power spectrum. Spectral efficiency describes how efficiently the allocated bandwidth is utilized or the ability of a modulation scheme to accommodate data, within a limited bandwidth [1]. *M*-ary

QAM permits the transmission of $K = \log_2 M$ bits during each symbol period. Since the use of *M*-ary symbols allows a K-fold increase in the data rate within the same bandwidth, then for a fixed data rate, use of *M*-ary QAM reduces the required bandwidth by factor K [2]. Combing spectrally efficient *M*-ary QAM with channel sharing in time is important for efficiently using the bandwidth resources in cost-effective wireless access networks.

1.2 Motivation

Since the ultimate task of the receivers is to produce an accurate replica of the transmitted symbol sequence, synchronization plays an important role for proper detection. Synchronization concerns the recovery of the reference parameters from the received signal and the use of these parameters to achieve demodulation and detection of the data from the signal [2]. Synchronization functions include carrier recovery and symbol timing recovery. When coherent detection is used, knowledge of both the frequency and phase of the carrier is necessary at the receiver. The estimation of carrier frequency and phase is called *carrier recovery* or *carrier synchronization* [3]. In this thesis we focus on the recovery of carrier frequency offset and phase offset. The symbol timing is assumed perfectly synchronized at the receiver.

Channel sharing in time involves "*burst-mode*" operation. Burst-mode communication varies from traditional continuous-mode communication in that data is transmitted in bursts or packets rather than in a continuous data stream. The burst format for a typical data packet is given in Figure 1.2. A so-called preamble is a set of

known modulation symbols, usually added to the user data packet at the transmitter with the intention of assisting the receiver in acquisition.

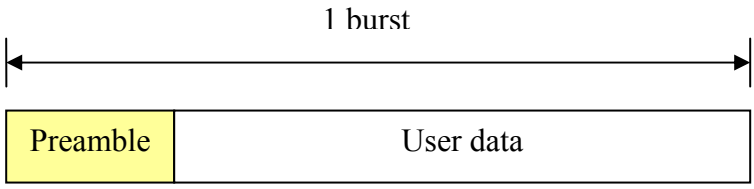

Figure 1.2 Burst format for a typical data packet

In burst-mode communications, fast, reliable, and efficient estimation of demodulator reference parameters is a key issue as the receivers must be able to correctly synchronize on very short period of bursts. Generally speaking, a preamble is used to achieve fast acquisition and reliable estimation. Provided that the synchronization parameters are extracted from the random data solely, the acquisition time length of common estimation structures may be too long [4]. In addition, the estimates produced by the synchronizer are also not accurate enough to perform reliable data detection, so that information symbols transmitted during acquisition are lost. For these reasons, it is necessary for burst-mode transmission to employ a preamble of training symbols which precedes the actual information symbols. On the other hand, preamble symbols consume bandwidth and power that are not used to convey digital information [4]. A separate acquisition preamble for each burst is an overhead that reduces the transmission throughput. Ideally, the preamble should be made as small as possible in order for the burst-mode transmission to be efficient.

The design of carrier synchronizers for burst-mode is very critical due to the burst nature of this type of communication system. The acquisition time, which is required at the start of every burst, must be short compared to the data portion of the burst to maintain efficient data throughput. Thus, the burst-mode demodulator requires a special acquisition process that is able to *quickly* estimate the synchronization parameters. Also, synchronization must be highly reliable on a burst-by-burst basis.

In the case of short burst mode, it may be sufficient to yield a single estimate of the synchronization parameters for each individual burst. However in the case of long burst mode, which is being considered in this thesis, the fluctuation of the synchronization parameters over the burst cannot be ignored, the synchronizer has to make multiple carrier phase estimates per burst, in order to track the variations of the synchronization parameters.

1.3 Objectives

Based on the above motivation, the goal of this research is to develop a fast carrier recovery system for coherent demodulation of burst-mode 16-QAM. To achieve this final goal, there are four main objectives in the research work:

- To investigate potential methods for rapid carrier recovery through extensive literature survey and choose suitable methods for burst-mode communications
- To develop rapid carrier synchronization algorithms for 16-QAM signals in AWGN environment

- To model and simulation the proposed carrier recovery system using Matlab®
- To evaluate and characterize the performance of the proposed estimators in burst-mode operation in the presence of non-ideal conditions (with frequency offset, phase offset, and additive white Gaussian channel noise)

1.4 Literature Review

Focusing on the issue of carrier recovery, a number of methods are considered. Traditional methods such as phase-locked loop (PLL, e.g. Costas loop) and decision directed (DD) methods [5] are widely used. Since these loops possess feedback, they may, in fact, suffer from "hang-up" phenomenon, that is, a prolonged dwell at large phase errors, thus not being able to provide rapid acquisition [6][7]. As a result, these synchronizers are not applicable if carrier frequency and phase offsets are quickly varying, or if the information is transmitted in bursts and must be obtained quickly as is the case for a TDMA scheme. The *feedforward* carrier offset estimation methods, which do not exhibit "hang-up", are likely more promising and are therefore used in this research as methods to potentially achieve fast carrier frequency offset and phase offset estimation.

It is very common that quadrature phase shift keying (QPSK), $\pi/4$ QPSK, or $\pi/4$ differential quadrature phase shift keying (DQPSK) is used as a modulation technique in burst-mode communications, because such modulation has the advantage that the envelope of the modulated signal is constant and is robust to the distortion. Carrier recovery algorithms for burst-mode have been well documented for QPSK or

$\pi/4$ QPSK modulation scheme [8][9][10]. 16-QAM scheme, which is more susceptible to noise and distortion than simpler modulation methods such as QPSK, has traditionally not been common for burst-mode communications. It is not surprising that very few research results have been published on 16-QAM scheme. Paper [9] suggests a decision-directed carrier frequency estimation. The algorithm performs a weighted average over the phase increments of two successive samples for estimating a signal frequency in a noisy environment. The simulation has verified that the bias is very small and diminishes with a larger roll-off factor. It is also found that the estimate is nearly unbiased as long as the influence of the mismatched filter is not too strong. However, the performance of the frequency estimate can be significantly improved if the autocorrelation distance used is greater than one step, as the method proposed in paper [10]. Paper [10] presents data-aided (DA) feedforward maximum-likelihood (ML) estimation algorithms for the carrier frequency and phase offsets in burst-mode QPSK communication systems. Experimental results demonstrate that the techniques provide a fast synchronization using a short preamble and low complexity. This research intends to apply the algorithms proposed in [10] to 16-QAM systems in carrier acquisition. Some modifications to the algorithms have been made and introduced in this thesis.

In the carrier tracking process, estimates are extracted from random user data instead of a known sequence (preamble). A great deal of analysis has been performed on the Viterbi and Viterbi (V&V) feedforward phase estimator, notably [11][12][13]. These papers clearly show the performance of this estimator assuming that the

frequency error is zero. Unfortunately, the estimator performance under the non-zero frequency error environment is not presented. In addition, the above estimation techniques are applied only to *M*-ary phase shifting keying (*M*-ary PSK) modulation schemes. Whether these techniques are applicable to 16-QAM is unknown. This research applies the V&V algorithm to 16-QAM schemes in carrier tracking. Some modifications specific to 16-QAM have been proposed. Also, the impact of frequency error on the phase tracking algorithm has been discussed in detail.

The major contributions of this research are the application of appropriate carrier recovery structure to burst-mode systems, the modification of the DA carrier frequency estimation algorithm proposed in the literature of [10], and also the slight modification of the V&V algorithm in non-data-aided (NDA) carrier phase synchronization. In this thesis, the basis of the estimation techniques is established, the estimators are developed and simulated, and the performance of all estimators is intensively analyzed.

1.5 Thesis Organization

The rest of this thesis is organized as follows:

Chapter 2 serves as the background explanation which is needed to understand the remainder of this thesis. The basic principle of wireless QAM modulation and demodulation is introduced. The optimum detector rule for 16-QAM signal corrupted

by additive white Gaussian noise (AWGN) is described and zero intersymbol interference (ISI) filtering technique is also discussed.

Chapter 3 introduces the carrier recovery theory and states some valuable design considerations for fast carrier synchronization for burst-mode communication. A suitable method of estimation and correction for burst-mode is decided. The block diagrams of carrier recovery system structures are also presented.

Chapter 4 develops carrier recovery algorithms for 16-QAM signals. The techniques include ML DA carrier frequency offset and phase offset estimations in the acquisition process, and an NDA carrier phase estimation in the tracking process.

Chapter 5 gives simulation results for the estimators presented in Chapter 4. The simulation is first set up according to the practical situation to evaluate the estimators developed. The bit error rate (BER) performance of these estimators is evaluated and compared.

Chapter 6 summarizes the research results, derives conclusions and gives some suggestions for future research.

Chapter 2

MODULATION AND DEMODULATION FOR THE AWGN CHANNEL

This chapter briefly introduces a digital wireless communication system and the rule of the optimum detection. It serves as a theory basis in order for readers to understand the remainder of this thesis better.

2.1 Overview

A communication link consists of three components: the transmitter, the channel, and the receiver. The transmitter element processes an information signal in order to produce a signal most likely to pass reliably and efficiently through the channel. This usually involves coding of the information signal to help correct for transmission errors, filtering of the signal to constrain the occupied bandwidth, modulation of a carrier signal by the information signal, and power amplification to overcome channel losses.

The transmission channel is loosely defined as the propagating medium or electromagnetic path between source and destination, for example cable, optical fibre, or atmosphere. The channel, in wireless communication, is the atmosphere which may add attenuation, delay, distortion, interference, and noise to the transmitted signal.

The receiver function is principally to reverse the modulation processing of the transmitter in order to recover the transmitted information signal, and attempts to compensate for any signal degradation introduced by the channel. This will normally involve amplification, filtering, demodulation, and decoding and in general is a more complex task than the transmit process.

2.2 Digital Modulation

In digital modulation, the information signals, whether audio, video, or data, are all digital. As a result, the digital information modulates an analog sinusoidal waveform carrier. The sinusoid has just three features that can be modified to carry the information: amplitude, frequency, and phase. Thus bandpass modulation can be defined as the process whereby the amplitude, frequency, or phase of the carrier, or a combination of them, is varied in accordance with the digital information to be transmitted [2]. If the amplitude, frequency, or phase of the carrier is altered by the digital information, then the modulation scheme is called amplitude shift keying (ASK), frequency shift keying (FSK), or phase shift keying (PSK), respectively.

2.2.1 QAM

Quadrature amplitude modulation (QAM) can be viewed as a combination of ASK and PSK. That means the digital information is carried in both the phase and the amplitude of the carrier signal. The *baseband equivalent representation*, $u_m(t)$, of the QAM signal can be expressed as

$$u_m(t) = (A_m^I + jA_m^Q)g(t) \qquad m = 1,2,...,M \quad (2.1)$$

where $A_m^I, A_m^Q \in \{\pm 1\Delta, \pm 3\Delta, ..., \pm(\sqrt{M}-1)\Delta\}$ (Δ is a constant whose value is determined by the average transmitted power) are referred to the inphase (I) and quadrature (Q) amplitudes corresponding to the M possible symbols in the two-dimensional space, as shown for 16-QAM in Figure 2.2, for example. The function $g(t)$ is a real-valued signal pulse whose shape influences the spectrum of the transmitted signal (The characteristics of $g(t)$ will be described in detail in Section 2.5.2.). The $u_m(t)$ in (2.1) can also be represented in polar form as

$$u_m(t) = A_m e^{j\theta_m} g(t) \qquad m = 1,2,...,M \quad (2.2)$$

where A_m and θ_m denote the amplitude and phase of the m^{th} symbol, and are given by

$$\begin{aligned} A_m &= \sqrt{\left(A_m^I\right)^2 + \left(A_m^Q\right)^2} \\ \theta_m &= \tan^{-1}\left(\frac{A_m^Q}{A_m^I}\right) \end{aligned} \qquad m = 1,2,...,M \quad (2.3)$$

The baseband signal described by (2.2) can be expressed as a bandpass signal, $s_m(t)$, which is chosen from one of M possible signalling waveforms

$$s_m(t) = \mathrm{Re}\left\{u_m(t)e^{j2\pi f_c t}\right\} = A_m\, g(t)\cos(2\pi f_c t + \theta_m) \quad m = 1,2,...,M \quad (2.4)$$

where f_c is the intermediate carrier frequency. Alternatively, the bandpass QAM signal in (2.4) can be expressed equivalently in terms of its quadrature components as

$$s_m(t) = A_m^I g(t)\cos 2\pi f_c t - A_m^Q g(t)\sin 2\pi f_c t \qquad m = 1,2,...,M \quad (2.5)$$

This representation leads to the most common functional representation of the QAM modulator, which is shown in Figure 2.1.

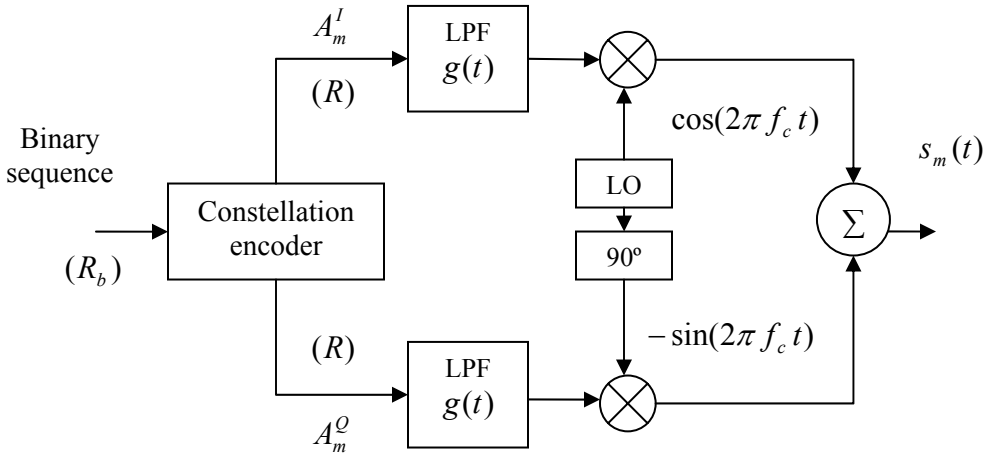

Figure 2.1 Typical QAM modulator

First, the input binary baseband sequence with bit rate R_b bits/second is encoded into two quadrature $\sqrt{M}$-level pulse amplitude modulation (PAM) signals, each having a symbol rate of $R = R_b / K$ symbols/second ($K = \log_2 M$). These two

components of I and Q are then filtered by pulse-shaping lowpass filters (LPFs), $g(t)$, to limit the transmission bandwidth. Finally the quadrature signals modulate the I and Q carriers for transmission. The transmitted bandpass signal $s(t)$, which is the summation of all symbols represented by the M possible signalling waveforms for QAM, can be expressed as [14]

$$s(t) = \mathrm{Re}\left\{\left(\sum_n I_n g(t-nT)\right)e^{j2\pi f_c t}\right\} \tag{2.6}$$

where transmission rate is $R = 1/T$ symbols/second and $\{I_n\}$ represents the discrete information-bearing sequence of symbols and is complex-valued for QAM.

Since the modulator output frequency is often lower than the desired transmission frequency, the modulator frequency must be up-converted to the appropriate radio frequency (RF) for transmission.

2.2.2 16-QAM

"16-QAM" results when $M = 16$ for *M*-ary QAM. QAM transmits $K = \log_2 M$ bits of information during each symbol period. For 16-QAM, there are 16 possible symbols each containing 4 bits, two bits for the I component and two bits for the Q component. The mapping of the bits into symbols is frequently done in accordance with the Gray code which helps to minimize the number of bit errors occurring for every symbol error. Because Gray-coding is given to a bit assignment where the bit patterns in adjacent symbols only differ by one bit [15], this code ensures that a single

symbol in error likely corresponds to a single bit in error. The rectangular constellation of a Gray-coded unfiltered 16-QAM signal is shown in Figure 2.2.

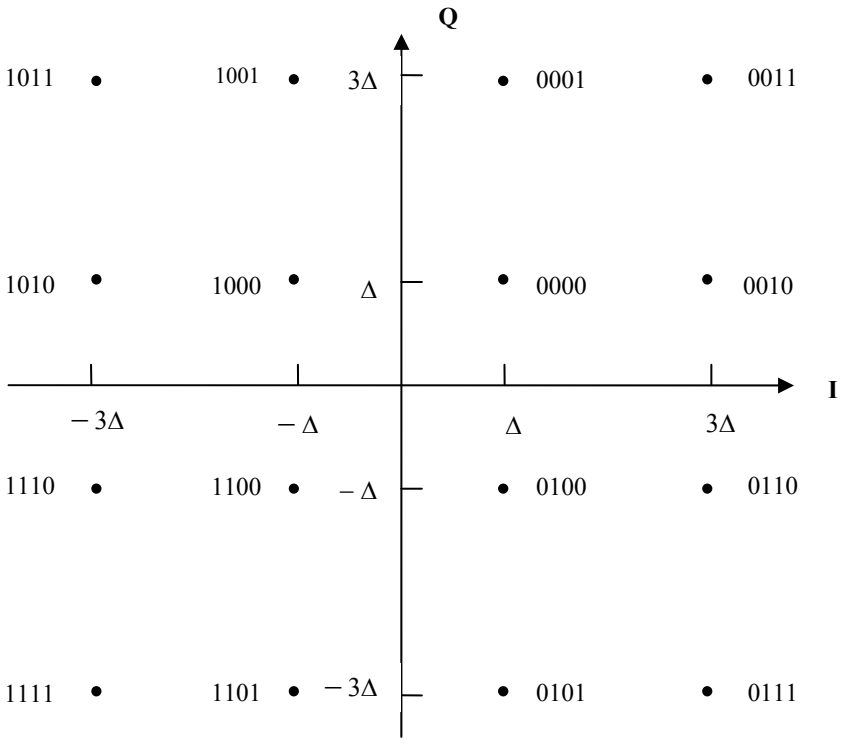

Figure 2.2 Rectangular constellation of a Gray-coded 16-QAM signal

The 16 symbols in the 16-QAM rectangular constellation diagram are equally spaced and independent, and each is represented by a unique combination of amplitude and phase.

Power Spectral Density for 16-QAM

The Fourier transform exists only for finite energy signals. For infinite energy signals, we usually use power spectral density (PSD) to characterize the distribution of signal power in the frequency domain. Instantaneous symbol transitions between the

constellation points of Figure 2.2 result in a wideband modulated signal with spectral components extending to infinity, as shown by the dotted line in Figure 2.3. To reduce the adjacent channel interference, the signal must be pre-filtered before transmission by a pulse-shaping filter to restrict the spectral occupancy to the main lobe. A commonly used realization of limiting the transmission bandwidth filter is the root raised cosine (RRC) filter.

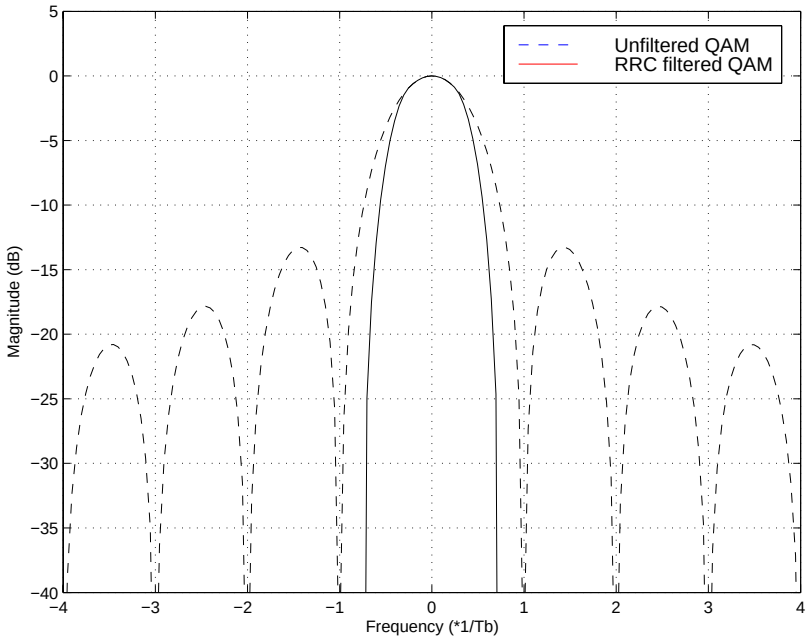

Figure 2.3 PSD for unfiltered and RRC pre-filtered 16-QAM

Figure 2.3 shows the effect of the RRC filter with a roll-off factor of 0.5 on the 16-QAM spectrum. We can see that pre-filtering removes the signal side lobes, which reduces the adjacent channel power radiation. More details on the specification and implementation of this filtering for the present research are provided in Section 2.5.2.

2.3 Channel

The channel is the propagating medium or electromagnetic path connecting the transmitter and the receiver. For a wireless channel, the characteristics are typically determined by the specific geography, atmospheric effects, objects in the channel, multipath effects, etc. The transmitter and receiver in this research are assumed to be fixed and communicate under line of sight (LOS) conditions, which means the transmitter and receiver are not moving and have a direct, unobstructed view of one another.

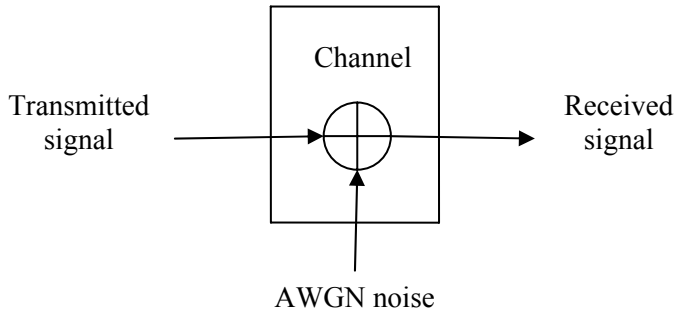

Figure 2.4 AWGN channel model

A reasonable assumption for a fixed, LOS wireless channel is the additive white Gaussian noise (AWGN) channel [14], which is flat and not "frequency-selective" as in the case of the fading channel. Particularly fast, deep frequency-selective fading as often observed in mobile communications is not considered in this thesis, since the transmitter and receiver are both fixed. This type of channel delays the signal and corrupts it with AWGN. The AWGN is assumed to have a constant PSD over the channel bandwidth, and a Gaussian amplitude probability density function. This

Gaussian noise is added to the transmitted signal prior to the reception at the receiver as shown in Figure 2.4.

The in-phase and quadrature components of the AWGN are assumed to be statistically independent, stationary Gaussian noise process with zero mean and two-sided PSD of $N_0/2$ Watts/Hz. As zero-mean Gaussian noise is completely characterized by its variance, this model is particularly simple to use in the detection of signals and in the design of optimum receivers. An example in Figure 2.5 shows how AWGN corrupts a 16-QAM signal with signal-to-noise ratio per bit (E_b/N_0) of 14 dB (E_b/N_0 is defined in Equation 2.13).

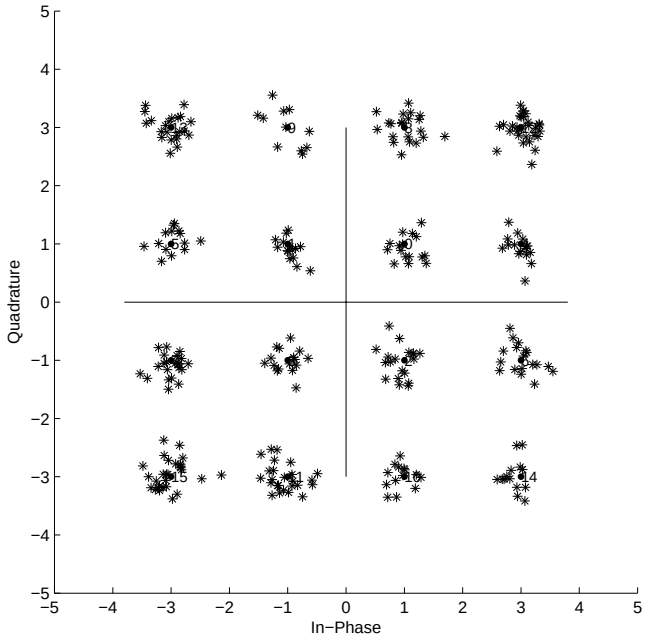

Figure 2.5 The scatter plot of 16-QAM signal corrupted by AWGN

It can be seen from Figure 2.5 that the noise causes symbols to "scatter" around the ideal constellation points. Since Gaussian noise samples are independent, the effect

on the detection process of a channel with AWGN is that the noise affects each transmitted symbol independently.

2.4 Coherent Demodulation

Since the information is carried in the phase and amplitude of the modulated carrier for the QAM signal, the receiver is assumed to be able to generate a reference carrier whose frequency and phase are identical to those of the carrier at the transmitter. When the receiver exploits knowledge of the carrier's phase to detect the signals, the process is called coherent demodulation/detection [2]. Figure 2.6 shows a block diagram of a QAM coherent demodulator.

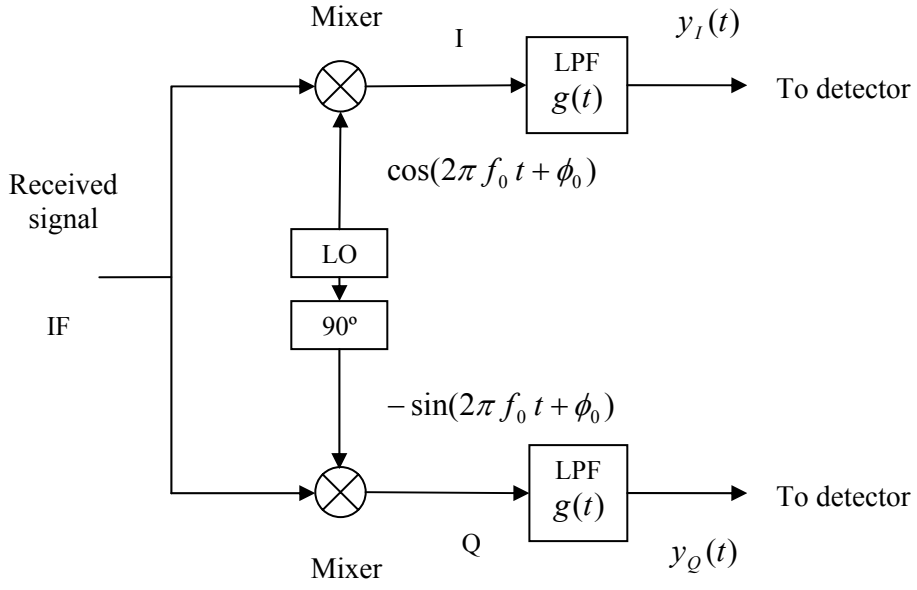

Figure 2.6 Block diagram of a QAM coherent demodulator

At the receiver, the received high frequency signal is first down-converted to a lower intermediate frequency (IF) before being further processed. The demodulator performs the majority of its work at an intermediate or baseband frequency. The mixer in the coherent demodulator converts the IF signal to a baseband signal, by multiplying the incoming IF signal with a locally generated carrier reference and the product is passed through a lowpass filter (LPF). The LPF removes the high-frequency components and selects the difference component from the mixer output. These LPFs also perform as matched filters whose impulse responses are matched to the transmitted signal to provide the maximum signal-to-noise ratio (SNR) at their output [14]. Then detectors decide which of the possible signal waveforms was transmitted from the output of the LPFs.

Assuming that Gaussian noise is the only channel disturbance, the received signal, $r(t)$, can be expressed as

$$r(t) = s(t) + v(t) \tag{2.7}$$

where $s(t)$ denotes the transmitted signal and $v(t)$ refers to the additive noise. Ignoring the noise, $r(t)$ is simplified as

$$r(t) = u_I(t)\cos(2\pi f_c t + \phi_c) - u_Q(t)\sin(2\pi f_c t + \phi_c) \tag{2.8}$$

where $u_I(t)$ and $u_Q(t)$ are the I and Q amplitudes of the information-bearing signal of the carrier (recall equation 2.1), f_c and ϕ_c are the carrier frequency and phase. This signal is demodulated by two quadrature reference carriers

$$c_I(t) = \cos(2\pi f_0 t + \phi_0)$$
$$c_Q(t) = -\sin(2\pi f_0 t + \phi_0) \tag{2.9}$$

where f_0 and ϕ_0 are the frequency and phase of the locally generated carrier. Multiplication of $r(t)$ with $c_I(t)$ followed by lowpass filtering yields the I component

$$y_I(t) = \frac{1}{2}u_I(t)\cos[2\pi(f_c - f_0)t + (\phi_c - \phi_0)] - \frac{1}{2}u_Q(t)\sin[2\pi(f_c - f_0)t + (\phi_c - \phi_0)] \tag{2.10}$$

Similarly, multiplication of $r(t)$ by $c_Q(t)$ followed by lowpass filtering yields the quadrature component

$$y_Q(t) = \frac{1}{2}u_Q(t)\cos[2\pi(f_c - f_0)t + (\phi_c - \phi_0)] + \frac{1}{2}u_I(t)\sin[2\pi(f_c - f_0)t + (\phi_c - \phi_0)] \tag{2.11}$$

We can see from expression (2.10) and (2.11) that if $f_c = f_0$ and $\phi_c = \phi_0$, the output of QAM demodulator is same as the transmitted baseband signal $u_I(t)$ and $u_Q(t)$; otherwise, the phase error $2\pi(f_c - f_0)t + (\phi_c - \phi_0)$ will reduce the signal level in voltage by the factor $\cos[2\pi(f_c - f_0)t + (\phi_c - \phi_0)]$ and in power by a factor $\cos^2[2\pi(f_c - f_0)t + (\phi_c - \phi_0)]$. Also there is cross-talk interference from the I and Q components. Since the average power levels of $u_I(t)$ and $u_Q(t)$ are similar, a small phase error causes a large degradation in performance. Hence, the phase accuracy requirements for QAM are very high.

Under ideal operating conditions, the local oscillator (LO) that generates the carrier signal for demodulation at the receiver is identical to that in the transmitter both in frequency and phase. But obtaining sufficiently stable free-running oscillators in both the transmitter and receiver units is not possible. First of all, the LO at the receiver is generally not synchronous in phase with that at the transmitter. Furthermore, the two oscillators may be drifting slowly with time. A reasonable cost-effective crystal oscillator may have a stability of 1 ppm (part per million) over a given temperature range. If we consider the case of a cellular radio modem operating with a carrier of 1 GHz, the oscillators at each of the link could have a frequency error of $\pm(1\times10^{-6})\times(1\times10^{9}) = \pm1$ kHz. If we could ensure that both transmit and receiver carrier oscillators begin with the same phase, then we expect the phase error between them to reach 360º after $1/2000 = 0.5$ ms. It is clear that simply achieving a correct starting phase will not allow us to ensure adequate coherency for more than a few microseconds. In this application, it is necessary to find a method of correcting the receiver carrier oscillator frequency and phase to match that of the transmitted signal. This process is termed *carrier recovery*. A more detailed discussion of carrier recovery will be presented in the following chapters.

2.5 Performance of the Optimum Detector

The ultimate task of receivers is to produce an accurate replica of the transmitted symbol sequence. The signal detector that follows the matched filter in the receiver must decide what possible signal was transmitted. The optimum detector is designed

to minimize the probability of error in the presence of the system and channel impairments. An important measure of modem performance is the *probability of error*. The probability of the detector making an incorrect decision is termed the probability of symbol error [2]. The probability of a symbol error for the *M*-ary QAM system in the presence of AWGN as a function of E_b/N_0 is obtained as [16]

$$P_s = 2\left(1-\frac{1}{\sqrt{M}}\right)erfc\left(\sqrt{\frac{3K}{2(M-1)}\left(\frac{E_b}{N_0}\right)}\right) \cdot\left[1-\frac{1}{2}\left(1-\frac{1}{\sqrt{M}}\right)erfc\left(\sqrt{\frac{3K}{2(M-1)}\left(\frac{E_b}{N_0}\right)}\right)\right] \tag{2.12}$$

where $K=\log_2 M$ and E_b/N_0 denotes the ratio of the bit energy E_b to noise power spectral density N_0. It is an expression of signal-to-noise ratio, S/N, normalized by bandwidth, B, and bit rate, R_b, denoted by [2]

$$\frac{E_b}{N_0}=\frac{S}{N}\left(\frac{B}{R_b}\right) \tag{2.13}$$

The dimensionless ratio E_b/N_0 is a standard quality measure for digital communication system performance. Therefore, required E_b/N_0 can be considered a metric that characterizes the performance of one system versus another; the smaller the required E_b/N_0, the more efficient is the detection process for a given probability of error.

In fact the user is more concerned with the probability of bit error than symbol error as this directly impinges on the integrity of the data sent to the user. For a binary system, bit error and symbol error are identical as each symbol error corresponds to a single bit error. For *M*-ary systems ($M > 2$), however, this does not hold true. In practice, some symbols are more likely to be detected in error than others, depending on how close or similar the symbols are to the correct symbol.

Since the error caused solely from AWGN will most likely push the decision point into an adjacent symbol for useful operating levels of E_b/N_0, we can make an assumption that the detection process will only mistake symbols for those adjacent to the correct symbol. When a Gray-coding is used in mapping, we can infer that the bit error probability, P_b, will be given approximately by the symbol error probability, P_s, divided by the number of bits K in each symbol [15], that is

$$P_b \approx \frac{1}{K} P_s \tag{2.14}$$

where $K = \log_2 M$.

2.6 Filtering and Intersymbol Interference

Pre-filtering allows the transmitted bandwidth to be significantly reduced without losing the content of the digital data. This improves the spectral efficiency of the signal, as was mentioned in Section 2.2.2. On the other hand, filtering results in the symbols spreading in time. This spreading causes part of the symbol energy to overlap

with neighbouring symbols, which is called intersymbol interference (ISI). ISI can significantly degrade the ability of the data detector to differentiate a current symbol from the diffused energy of adjacent symbols. This can lead to detection errors and will reduce the BER performance.

To get zero ISI, the overall system filter transfer function must be what is termed a "Nyquist" frequency response. For this type of filter, the time response goes through zero with a period that exactly corresponds to the symbol spacing. By sampling the symbol sequence at the precise symbol times point, the energy spreading from the adjacent symbols does not affect the value of the present symbol, and ISI is thus eliminated. A commonly used realization of the Nyquist filter is a raised cosine (RC) filter.

The RC filter impulse response, $h_{RC}(t)$, and frequency response, $H_{RC}(f)$, can be expressed mathematically as [15]

$$h_{RC}(t) = \operatorname{sinc}(\pi t/T)\frac{\cos(\pi r t/T)}{1-(2r t/T)^2} \tag{2.15}$$

and

$$H_{RC}(f) = \begin{cases} T & |f| \le \dfrac{1-r}{2T} \\ \dfrac{T}{2}\left[1+\cos\left(\dfrac{\pi T}{r}\left(|f|-\dfrac{1-r}{2T}\right)\right)\right] & \dfrac{1-r}{2T} < |f| \le \dfrac{1+r}{2T} \\ 0 & \dfrac{1+r}{2T} < |f| \end{cases} \tag{2.16}$$

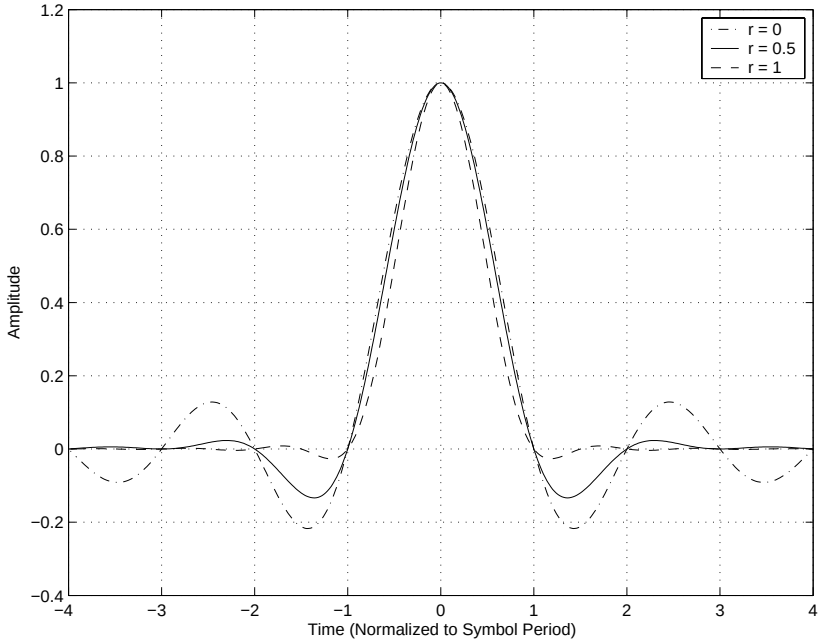

Figure 2.7a Impulse response of the RC filter for different roll-off factors

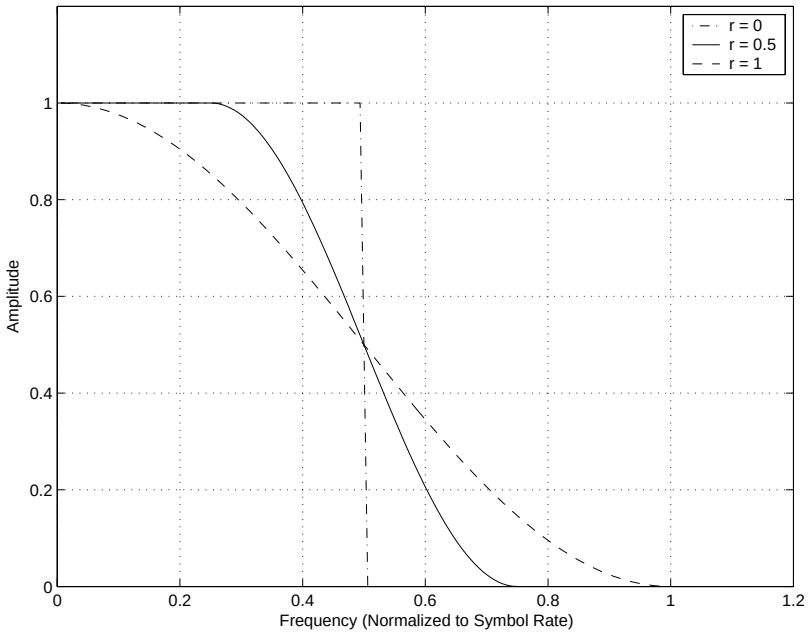

Figure 2.7b Frequency response of the RC filter for different roll-off factors

where r is called the roll-off factor, which determines the filter bandwidth and takes values in the range $0 \le r \le 1$. It represents a trade-off between the sharpness of the transition band of the filter and the magnitude of the ringing of the impulse response of the filter. T is the symbol period, which is inversely proportional to symbol rate R, i.e., $T = 1/R$. The impulse response and the frequency response of the RC filter is illustrated in Figure 2.7a and Figure 2.7b for three values of r (r = 0, 0.5, 1).

We can notice from Figure 2.7a that time response of the RC filter does go through zero with a period that exactly corresponds to the symbol spacing. Adjacent symbols do not interfere with each other at the symbol times because the response equals zero at all symbol times except the centre (desired) one. This type of filter heavily filters the signal without blurring the symbols together at the symbol times. This is important for transmitting information without errors caused by ISI. Note that ISI does exist at all times except the symbol (decision) times.

Usually this RC filter is split equally into a root raised cosine (RRC) filter pair, with one in the transmitter, performing the pulse shaping to constrain the modulated signal bandwidth, and the other in the receiver, performing matched detection for optimizing the SNR of a known signal in the presence of AWGN. The RRC filter is so called because the transfer function is exactly the square root of the transfer function of the RC filter. The impulse response, $h_{RRC}(t)$, and the frequency response, $H_{RRC}(t)$, of the RRC filter is given by [15]

$$h_{RRC}(t) = \frac{4r}{\pi\sqrt{T}} \frac{\cos\left[(1+r)\pi t/T\right] + \dfrac{1}{4rt/T}\sin\left[(1-r)\pi t/T\right]}{1-(4rt/T)^2} \tag{2.17}$$

and

$$H_{RRC}(f) = \begin{cases} \sqrt{T} & |f| \le \dfrac{1-r}{2T} \\ \sqrt{\dfrac{T}{2}\left[1+\cos\left(\dfrac{\pi T}{r}\left(|f| - \dfrac{1-r}{2T}\right)\right)\right]} & \dfrac{1-r}{2T} < |f| \le \dfrac{1+r}{2T} \\ 0 & \dfrac{1+r}{2T} < |f| \end{cases} \tag{2.18}$$

Figure 2.8a and 2.8b show the impulse response and frequency response of the RRC filter for a number of roll-off factors. The RRC filter bandwidth corresponding to root mean square (RMS) amplitude is $R/2$.

Inspecting these two pulse shapes of RC and RRC (Figure 2.7a and Figure 2.8a), we see that they have a similar appearance, but the RRC pulse makes slightly faster transitions, thus its spectrum does not decay as rapidly as the spectrum of the RC pulse. Another subtle but important difference is that the RRC pulse does not exhibit zero ISI (you can verify that the pulse tails in Figure 2.8a do not go through zero amplitude at the symbol times). However, if RRC filter is used at both the transmitter and the receiver, the product of these transfer functions being a raised cosine, will give rise to an output having zero ISI.

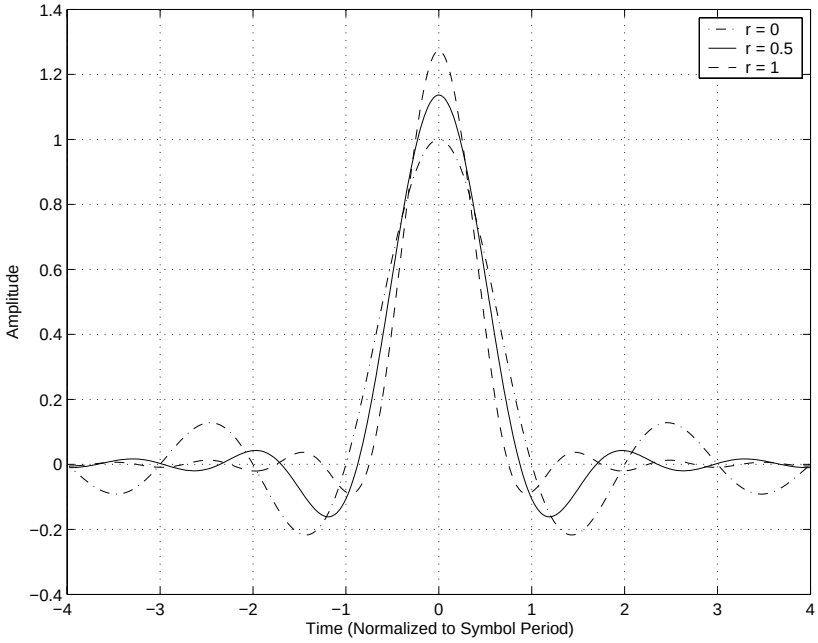

Figure 2.8a Impulse response of the RRC filter for different roll-off factors

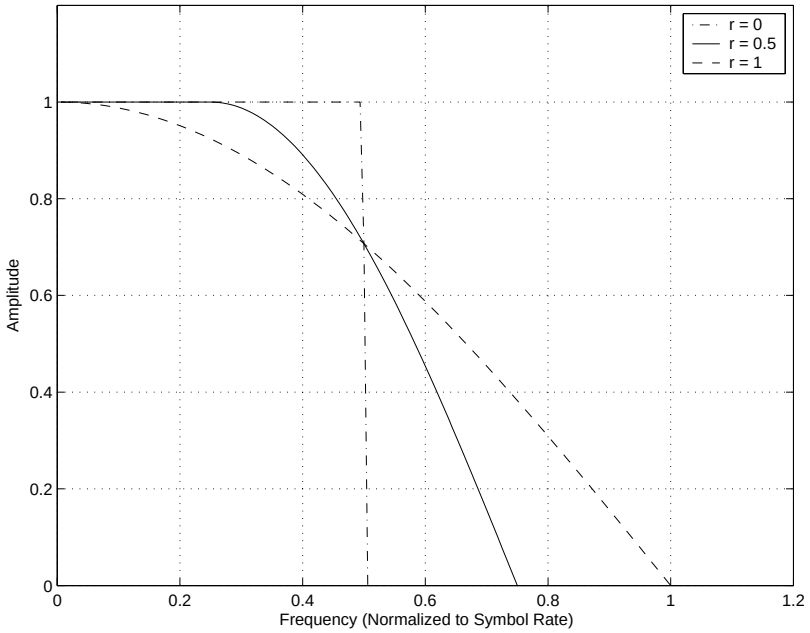

Figure 2.8b Frequency response of the RRC filter for different roll-off factors

2.7 Summary

The fundamentals of the modem in the wireless communication were briefly addressed in this chapter. Carefully choosing the modulation scheme for bandpass transmission is critical, because it may improve the bandwidth efficiency of bandpass data transmission. *M*-ary bandpass modulation techniques, particularly *M*-ary QAM, are widely used in wireless digital communication links. 16-QAM is used as the modulation technique in this research.

The signalling waveforms are passed through a channel that introduces AWGN. The coherent detection requires the receiver to synchronize the carrier's phase and frequency (carrier recovery) to detect the signals. The performance of the optimal detector in the presence of AWGN can be derived statistically, but typically assumes perfect synchronization.

Filtering improves the spectral efficiency of the transmitted signal. On the other hand, filtering can also create ISI. The importance of Nyquist filtering in establishing a theoretical minimum bandwidth for symbol detection without ISI is discussed.

Chapter 3

CARRIER RECOVERY SYSTEM DESIGN

This chapter aims at determining the carrier recovery method for burst-mode systems. Based on the method chosen, the carrier recovery system is designed and the system structures are also presented. It is clarified that "synchronization" in this thesis implies carrier synchronization only and not symbol timing synchronization, which is always assumed to be perfect in this research.

3.1 Carrier Recovery Description

As Section 2.4 described, when coherent detection is used, the receiver must exploit knowledge of both carrier frequency and phase to detect the signals. Carrier recovery typically entails two subsequent steps: in the first step carrier synchronization parameters are estimated, and in the second the receiving carrier signal is corrected according to the estimates made. These steps must be performed quickly and accurately in burst-mode.

3.1.1 Carrier Recovery Parameters

The carrier synchronization parameters include carrier frequency offset and carrier phase offset. *Carrier frequency offset* is mainly caused by two mechanisms – the frequency instability in either the transmitter or receiver oscillator, and the Doppler effect when the receiver is in motion relative to the transmitter. The former is generally the cause of the carrier frequency offset in a fixed wireless link as is the situation for this research. *Carrier phase offset* is the result of three major components in this application, namely, the phase instability in oscillators, the phase due to transmission delay, and thermal noise (such as AWGN).

Assuming that the frequency and phase of a carrier are f_c and ϕ_c, and the frequency and phase of a LO at receiver are f_0 and ϕ_0, then after the received signal mixed with the LO, the initial carrier frequency offset and phase offset may be created and can be modeled as

$$f = f_c - f_0 \tag{3.1}$$

and

$$\phi = \phi_c - \phi_o \tag{3.2}$$

We will see in Figure 3.1a that a carrier frequency offset f causes 16-QAM symbols to rotate with time by $e^{j2\pi ft}$, while Figure 3.1b shows a carrier phase offset ϕ results in a rotation of 16-QAM symbols by $e^{j\phi}$, where $\phi = 30^\circ$.

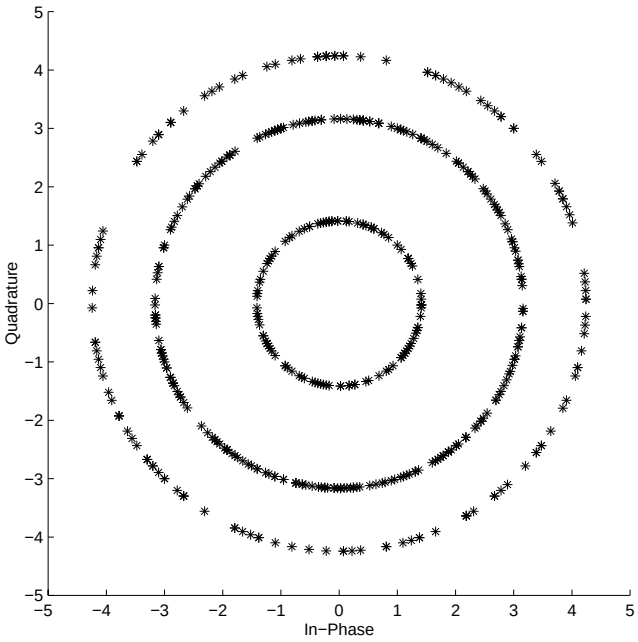

Figure 3.1a 16-QAM constellation with frequency offset

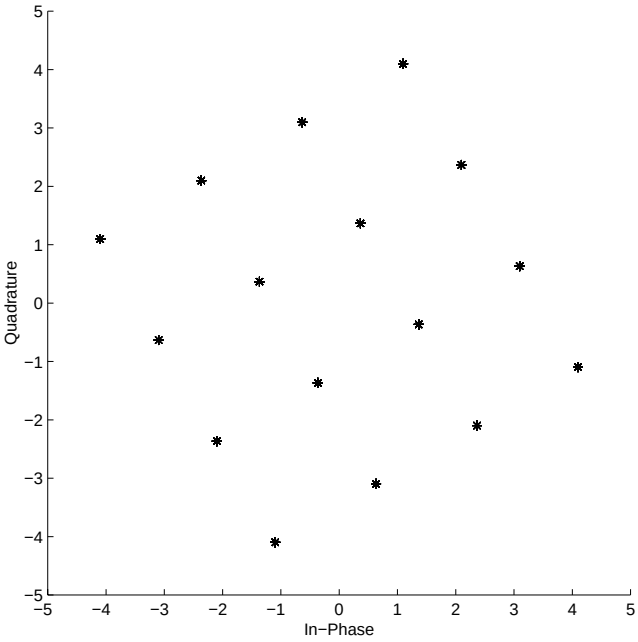

Figure 3.1b 16-QAM constellation with phase offset

It can be seen from Figure 3.1 that the 16-QAM constellation is seriously spoiled due to the frequency and phase offsets. Even a small frequency or phase offset may highly impair the symbol detection. 16-QAM symbols could not be correctly detected without proper compensation. For this reason, the receiver must be provided with accurate carrier frequency and phase estimates from the received signal itself by means of a carrier synchronizer, and then the received signal must be corrected according to the estimates made. Carrier frequency offset should be estimated and compensated prior to the phase offset compensation. This is because the initial carrier frequency offset can be large enough to cause phase rotation of a substantial part of a cycle in a single symbol and, as a result will prevent successful estimation of carrier phase offset.

3.1.2 Carrier Recovery Processes

Carrier recovery occurs in two subsequent phases of acquisition and steady-state tracking. At the start of signal reception, the synchronizer has no knowledge about the synchronization parameter values. After some processing of the received signal, the synchronizer is able to deliver accurate estimates of the synchronization parameters which are needed for reliable data detection. This transition from a large initial uncertainty about the synchronization parameters to a small steady-state estimation error variance is called *carrier acquisition* [4].

In the burst-mode carrier acquisition, the synchronizer performs the initial frequency and phase offset estimation during the preamble. At the end of the

preamble, the acquisition should be completed so that reliable data detection can start in the data portion of the burst. The performance of the acquisition is critical for any modem, but more so in this case because of the burst-mode setting. The synchronization parameters must be recovered quickly so that detection of the data portion of the burst may begin. In general, a preamble is used to accelerate acquisition; however, overhead must be kept low in order for the system to be efficient. To do this, the carrier acquisition system must be *fast*.

In the case of short burst communication, where the number of data symbols per burst is small, it may be sufficient to consider the carrier phase as constant over the entire burst. It is sufficient to produce a single carrier frequency and phase estimate per burst, and use these parameters for detecting all data symbols within the burst. However, in the case of long burst communication, the fluctuation of the synchronization parameters over the burst cannot be ignored, because the frequency offset estimated in the acquisition process is not perfectly accurate, and the *residual frequency error* will accumulate phase error with time and cause a loss of phase synchronization. It leads to severe problem in symbol detection. The carrier recovery system must make several estimates per burst so that the variations of the carrier phase over the burst can be tracked. This process is called *carrier tracking*. The estimates are extracted from the random data part of the burst in carrier tracking.

3.2 Design Considerations

The first problem of how to derive synchronization parameters in the receiver must be addressed. There are many ways to recover carrier offsets, but here we want to use the method suitable for burst-mode systems. Since fast and efficient estimation of carrier synchronization parameters is a key issue for burst-mode, the preamble and the synchronizer structure should be chosen carefully.

3.2.1 Preamble Selection

The acquisition process is usually aided by formatting the transmitted burst to include a *preamble*, which is a fixed sequence of symbols known to the receiver and which the receiver can use to form estimates. Preamble-based synchronization techniques are widely used today in communication systems as they have the advantage that the estimation process is much simpler and the performance is better at low SNR values or high frequency offset values.

The content of the preamble affects the acquisition performance. It is advisable that a preamble has the following properties:

- Periodically repeating sequences of modulation symbols
- A data sequence that makes the symbol transitions as obvious as possible,
- A unique word with good correlation properties

In most cases, it makes sense to restrict the symbols used in the preamble to either of two antipodal values. For 16-QAM, the preamble can be restricted to using only two points on opposite sides of the constellation. Allowing only two antipodal values simplifies the correlation problem, since the correlation is a sequence that is real rather than a complex.

The preamble length needed depends on the estimation algorithm being used for acquisition as well as the required system performance, such as how accurate the parameter estimates extracted from the preamble have to be and what "miss rate" and "false alarm" are acceptable for detection. The preamble length must reflect the following considerations:

- The longer the preamble, the more accurate the estimate is.
- Operating at higher E_b/N_0 allows the preamble to be shorter.
- Using more complex modulations (such as higher orders of QAM) will require longer preambles because estimates of carrier frequency must be more accurate.

The choice of the preamble length is a trade-off between the estimation accuracy and the transmission efficiency. Properly selecting the preamble can achieve fast and reliable synchronization in burst-mode systems.

3.2.2 Synchronizer Structure Selection

The carrier synchronization method can be categorized as *feedforward* (FF) and *feedback* (FB) according to how the estimates are extracted from the received signal. FF directly estimates the unknown parameters from the received signal before the signal is corrected in the phase rotator. The other category, FB, derives an estimate of error while feeding a corrective signal back to the phase rotator [4].

As it was mentioned before, the rapid carrier recovery is critical in burst transmission. Traditional FB synchronizers such as phase-locked loops (PLLs) have a small frequency capture range and need very long acquisition time when the frequency offset is much larger than the loop bandwidth (pull-in) or when the initial synchronization error is close to an unstable equilibrium point (hang-up) [6]. As a result, these synchronizers are not applicable if frequency and phase errors are quickly varying, or if the information is transmitted in bursts (as is the case for a TDMA scheme). For these cases, FF estimators are preferred to FB ones, because FF implementations are not plagued by some of the effects encountered with FB loops like hang-up. In addition, FF estimators have a larger estimation range and only require a small number of symbols for acquisition. The relevant information can be quickly collected at the receiver and FF estimators introduce no delay due to acquisition. Nevertheless, FB estimation is more suitable for continuous transmissions since it inherently has the ability to automatically track variations of the parameters instead of always starting the memoryless estimation process from burst to burst as FF structures do.

In addition, when a preamble is used to recover the reference parameters it is more important to have a FF structure, which allows these parameters to be estimated quickly, simultaneously and directly. For these reasons, FF structures are used in this research as a method to recover carrier parameters during carrier acquisition and tracking.

3.3 System Design

The overall carrier recovery system block diagram is given in Figure 3.2, according to the method described above.

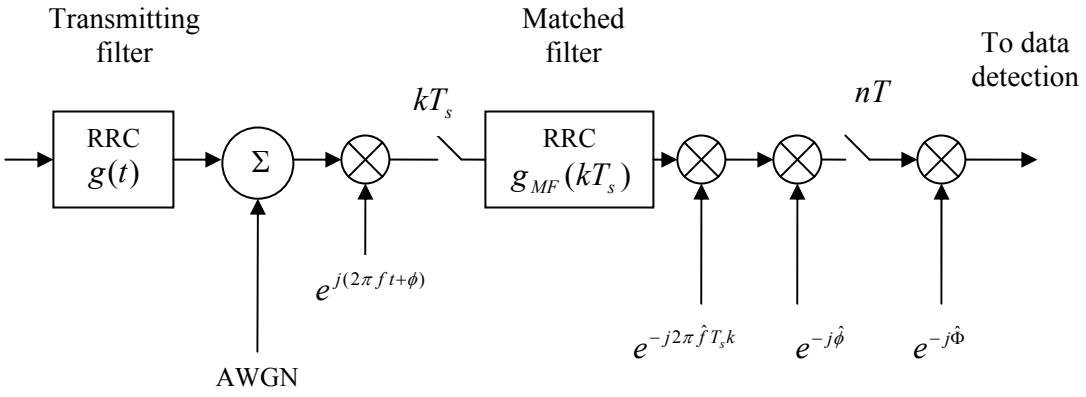

Figure 3.2 FF baseband carrier recovery system block diagram

In this digital receiver, the incoming noise corrupted signal is first coherently demodulated to a baseband signal, which may be subject to the frequency offset f and the phase offset ϕ. The estimation of f and ϕ ($\hat{f}$ and $\hat{\phi}$) in acquisition is based on the matched filter samples, which are obtained by oversampling of the received preamble sequence at sampling rate of $1/T_s$, a rate higher than the symbol rate (k is

the sampling index in Figure 3.2). The oversampling has two advantages: one is that symbol timing is not necessary to be recovered first; the other is that it reduces the number of preamble symbols needed and accelerates the speed of the acquisition, which is the most important issue in burst-mode communications.

After the received signal is adjusted according to the estimates made in preamble, the sampling rate is converted down to the symbol rate $1/T$ before the tracking starts. It is assumed that symbol timing is perfectly synchronized during data portion by taking samples at the instants of maximum eye opening to obtain one sample per symbol (n is the symbol index in Figure 3.2). The phase estimation ($\hat{\Phi}$) during the user data portion keeps reducing the fluctuation of the synchronization parameters and be ready for data detection. The details for the carrier acquisition estimator and carrier tracker will be presented in the rest of this section.

3.3.1 Carrier Acquisition Estimator

The carrier acquisition process, which includes carrier frequency offset estimation and correction as well as carrier phase offset estimation and correction, is performed digitally at the receiver end. Figure 3.3 shows the block diagram of the FF carrier acquisition estimator.

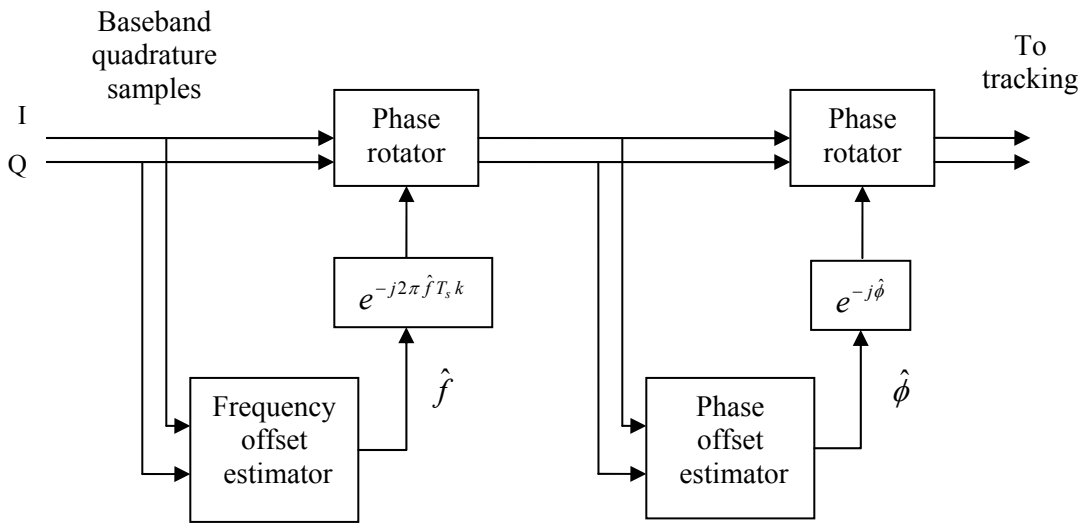

Figure 3.3 Block diagram of FF carrier acquisition estimator

The baseband quadrature samples are obtained by oversampling of a known preamble. The carrier acquisition estimator uses these samples to acquire the initial frequency offset estimate $\hat{f}$ and phase offset estimate $\hat{\phi}$. The estimates of frequency offset and phase offset are treated as sequential tasks – the frequency offset is estimated and the signal compensated before signal entering the phase estimator. The frequency offset can be compensated by multiplying the baseband samples by a complex number $\exp\left(-j2\pi\hat{f}(kT_s)\right)$ in the phase rotator. Similarly, the phase offset is corrected by multiplying the frequency synchronizer output by $\exp\left(-j\hat{\phi}\right)$ after the $\hat{\phi}$ is acquired.

3.3.2 Carrier Tracker

Once the acquisition phase in the preamble has ended, the tracking phase for the data portion of the burst starts: a tracking loop gives multiple estimates of the carrier

phase using the values estimated in the acquisition phase as the initial values, and thus allowing a considerable reduction in the transient time loops. The block diagram of the FF carrier tracker used in this research is shown in Figure 3.4.

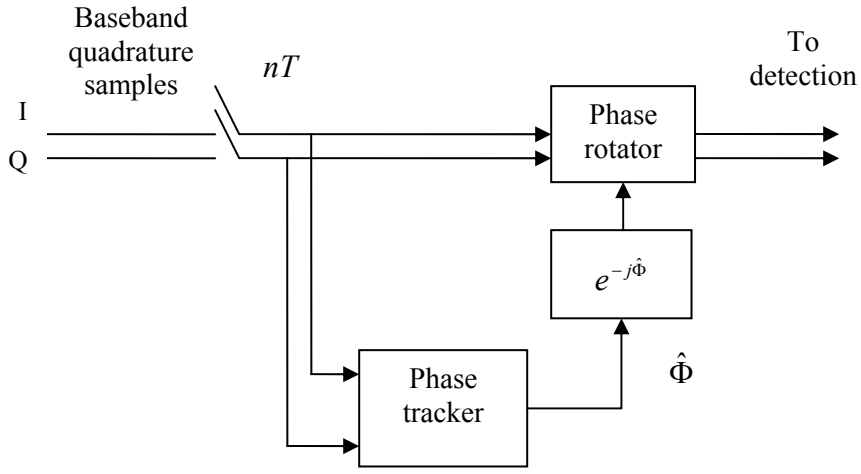

Figure 3.4 Block diagram of FF carrier tracker

The sampling rate is first converted down to the symbol rate T with the aid of the symbol timing knowledge. Then the carrier tracker estimates and adjusts the phase error in the random user data portion. This phase error is mainly caused by inaccurate frequency offset estimate $\Delta f = f - \hat{f}$ and inaccurate phase offset estimate $\Delta\phi = \phi - \hat{\phi}$ in the acquisition phase. The Δf and $\Delta\phi$ can be compensated by a time-variant phase estimate $\hat{\Phi}(nT) = \Delta\phi + 2\pi\Delta f(nT)$. The output symbols from the carrier synchronizer are further processed in the detection/decoding unit to decide what symbols have been transmitted.

It can be found that a good estimate of the initial carrier frequency offset in the acquisition part is critical. This is because the following phase estimates in tracking depend on the accuracy of the initial frequency estimation.

3.4 Summary

All digital communication systems require some degree of synchronization to incoming signals by the receivers. In this chapter the fundamentals of carrier synchronization are discussed. The discussion begins with the basic parameters of carrier synchronization required for coherent reception – frequency and phase synchronization. The carrier recovery process is often divided into two modes, namely, acquisition and tracking. The frequency and phase acquisition process brings the local frequency and phase into a coarse alignment with those of the incoming signal and the phase tracking process reduces and maintains the residual frequency and phase errors within a small tolerance range.

Since fast and efficient estimation of demodulator reference parameters is critical for burst-mode, it is desirable to find an acquisition method for the burst modem to be able to receive the burst with a performance that approaches theory and with as rapid estimation as possible. Generally speaking, a preamble is used to accelerate acquisition; however, overhead must be kept low in order for the system to be efficient. Traditional methods of synchronization using PLL have demonstrated reduced performance when operated in burst-mode systems due to exhibiting hang-up phenomenon. Therefore, the reference parameter recovery for burst-mode is generally

achieved by using feedforward technique. Based on above considerations, the block diagrams of carrier recovery system are also presented in this chapter.

Chapter 4

CARRIER RECOVERY ALGORITHMS

This chapter presents the maximum likelihood (ML) based feedforward digital estimation algorithms for determining the carrier offsets for 16-QAM signals in the AWGN environment. The techniques include DA carrier frequency and carrier phase estimations in the acquisition process, and NDA carrier phase estimation in the tracking process.

4.1 The Received Signal Model

For a modulated carrier transmitted over an AWGN channel, the equivalent baseband received signal can be expressed as

$$r(t) = u(t)e^{j(2\pi f t+\phi)} + v(t) \tag{4.1}$$

where $u(t)$ is the baseband equivalent signal of 16-QAM, f is the carrier frequency offset to be estimated in Hertz , ϕ is an unknown carrier phase offset, and $v(t)$ is an AWGN with zero mean and double-sided power spectral density (PSD) of $N_0/2$.

If signal $r(t)$ is sampled at a rate $1/T_s$ and after matched filtering, it results in

$$r_k \overset{\Delta}{=} r(kT_s) = u_k e^{j(2\pi f T_s k+\phi)} + v_k = s_k(f,\phi) + v_k \qquad k = 1,2,...,N \quad (4.2)$$

where k is the sample index, and N is the number of samples in the observation window. The sampling rate $1/T_s$ is equal to an integer multiple of the symbol rate $1/T$. The oversampling and matched filtering produces a set of samples of the received signal, $[r_1, r_2, ..., r_N] \equiv \mathbf{r}$, which contains all the information in the received signal waveform and is sufficient statistics to represent $r(t)$ [4]. The frequency offset f may be rewritten more conveniently as an incremental phase error normalized to the sampling rate, $\Omega = 2\pi f T_s$. The carrier frequency and phase offsets are assumed unknown but non-random parameters, and constant for the duration of the burst. The symbol timing is assumed perfectly known at the receiver. We let ψ denote the parameter vector $\{f, \phi\}$, so that $s_k(f,\phi)$ is simply denoted by $s_k(\psi)$.

In this thesis, the frequency and phase offsets are assumed constant over duration of the burst. However, we should be aware that these parameters are always time variant. But the time scale on which changes of these parameters are observable is much larger than the time scale necessary to express the symbol duration. Therefore, it is reasonable to consider these synchronization parameters to be constant over a number of symbols. This assumption greatly eases the systematic derivation of synchronizers.

4.2 ML Parameter Estimation

4.2.1 MAP and ML

There are basically two criteria that are widely applied to signal parameter estimation: the *maximum a posteriori probability* (MAP) criterion and the *maximum likelihood* (ML) criterion [14]. In the MAP criterion, the parameter ψ we want to estimate is regarded as random variable, and characterized by an a priori probability density function (pdf) $p(\psi)$. In the ML criterion, the parameter ψ is treated as deterministic but unknown.

Since we may represent $r(t)$ by a set of samples $\{r(kT_s)\}$, the joint pdf of the random variable $[r_1, r_2, ..., r_N]$ can be expressed as $p(\mathbf{r}|\psi)$. Then, the ML estimate of ψ is the value that maximizes $p(\mathbf{r}|\psi)$. On the other hand, the MAP estimate is the value of ψ that maximizes the a posteriori pdf

$$p(\psi|\mathbf{r}) = \frac{p(\mathbf{r}|\psi)p(\psi)}{p(\mathbf{r})} \tag{4.3}$$

However, the characterization of the behaviour of the parameter through its pdf is not always available. Estimation methods of the ML approach have been designed to solve this issue as long as they do not call upon the a prior pdf of the parameter. This is made possible by assuming that the parameter is uniformly distributed or constant over the span of possible values. In such a case, the value of ψ that maximizes $p(\mathbf{r}|\psi)$ also maximizes $p(\psi|\mathbf{r})$. Therefore, MAP and ML estimates are identical

[14]. In this thesis, the parameter ψ is treated as unknown, but deterministic. Hence, the ML criterion is adopted. As a result, if a preamble of known symbols is transmitted prior to sending the useful data, during the preamble, the synchronization parameters can be estimated by

$$\hat{\psi}(\mathbf{a}) = \arg\left\{ \max_{\psi} p(\mathbf{r} \mid \mathbf{u} = \mathbf{a}, \psi) \right\} \tag{4.4}$$

where $\mathbf{a}$ represents a vector of preamble samples, $\mathbf{u}$ denotes a set of random symbol samples, and $\arg(\cdot)$ represents the angle. Equation (4.4) leads to the data-aided (DA) estimation rule. Another possibility is to actually perform the averaging operation for all possible 16-QAM symbols to remove the data dependency

$$p(\mathbf{r} \mid \psi) = \sum_{all\ \mathbf{u}} p(\mathbf{r} \mid \mathbf{u}, \psi) p(\mathbf{u}) \tag{4.5}$$

This leads to the class of non-data-aided (NDA) synchronization algorithms

$$\hat{\psi} = \arg\left\{ \max_{\psi} p(\mathbf{r} \mid \psi) \right\} \tag{4.6}$$

4.2.2 Likelihood Function

As mentioned before, the carrier frequency offset and phase offset to be estimated are regarded as unknown and non-random parameters. This suggests the ML estimator as the preferred strategy. The derivation of likelihood function will be introduced next.

Since the additive noise $v(t)$ is statistically independent Gaussian with zero-mean and variance of $N_0/2$, its components in the expansion vector are statistically independent and jointly Gaussian, so that the joint pdf of a set of N samples $\{r_k\}$ may be expressed as [14]

$$p(\mathbf{r}\,|\,\psi) = (\pi N_0)^{-N/2} \exp\left\{-\sum_{k=1}^{N} \frac{[r_k - s_k(\psi)]^2}{N_0}\right\} \tag{4.7}$$

where

$$\begin{aligned} r_k &= \int_{T_0} r(t)\,\delta(t - kT_s)\,dt \\ s_k(\psi) &= \int_{T_0} s(t,\psi)\,\delta(t - kT_s)\,dt \end{aligned} \tag{4.8}$$

where T_0 represents the integration interval in the expansion of $r(t)$ and $s(t;\psi)$, and $\delta(\cdot)$ is impulse function. The maximization of $p(\mathbf{r}\,|\,\psi)$ with respect to the signal parameters ψ is equivalent to the maximization of the *likelihood function*

$$\Lambda(\psi) = \exp\left\{-\frac{1}{N_0}\sum_{k=1}^{N} |r_k - s_k(\psi)|^2\right\} \tag{4.9}$$

The ML estimate is the value of the parameter that maximizes the likelihood function. From (4.9), it can be interpreted as the value of the parameter which minimizes the distance between the received signal $r(t)$ and the noiseless signal $s(t;\psi)$ assuming ψ. Expanding the binomial term in (4.9), this function becomes

$$\Lambda(\psi) = \exp\left\{ -\frac{1}{N_0}\sum_{k=1}^{N}|r_k|^2 + \frac{2}{N_0}\mathrm{Re}\left[\sum_{k=1}^{N} r_k s_k^*(\psi)\right] - \frac{1}{N_0}\sum_{k=1}^{N}|s_k(\psi)|^2 \right\} \quad (4.10)$$

Note that the first term of the exponential factor does not involve the signal parameter ψ. The third term, $|s_k(\psi)|^2$, is a constant equal to the signal energy for any value of ψ. Only the second term, which involves the cross-correlation of the vector $\{r_k\}$ with the vector $\{s_k(\psi)\}$, depends on the choice of ψ. Therefore, the likelihood function $\Lambda(\psi)$ may be expressed as

$$\Lambda(\psi) = C\exp\left\{ \frac{2}{N_0}\mathrm{Re}\left[\sum_{k=1}^{N} r_k s_k^*(\psi)\right] \right\} \quad (4.11)$$

where C is a constant independent of ψ, and the asterisk denotes complex conjugate. Searching for the ML estimate is not easy due to the exponential function in (4.11). However, since the logarithm is a monotonic function of its argument, the value which maximizes $\Lambda(\psi)$ also maximizes $\log\Lambda(\psi)$. So, usually, instead of dealing with the exponential function appearing in the likelihood function, one prefers to use its logarithm. Taking the logarithm, we get the log-likelihood function

$$\Lambda_L(\psi) = \frac{2}{N_0}\mathrm{Re}\left[\sum_{k=1}^{N} r_k s_k^*(\psi)\right] \quad (4.12)$$

Notice that in defining $\Lambda_L(\psi)$, the constant term $\ln C$ is ignored. The ML estimate $\hat{\psi}$ is defined as the value of ψ that maximizes logarithm of the likelihood function $\Lambda_L(\psi)$ (or the likelihood function $\Lambda(\psi)$) [3].

In the ML estimation, the estimate is extracted by observing a block of received data, referred to as the *observation window*. In the acquisition process, the length of this observation window is selected in accordance with acquisition time requirements. The preferred tracking is usually in the form of a tracking loop where the parameter estimates are being continuously updated. The update speed is directly related to the observation window.

4.2.3 ML Condition

ML estimates are theoretically derived from the maximization of the likelihood function. A necessary condition for this maximum can be obtained by differentiating the logarithm of the likelihood function with respect to the unknown vector parameter ψ and setting the derivative to zero

$$\left.\frac{\partial \Lambda_L(\psi)}{\partial \psi}\right|_{\psi=\hat{\psi}} = 0 \tag{4.13}$$

The ML estimate $\hat{\psi}$ can be found to be the solution of the equation (4.13) in terms of $\mathbf{r}$ [3]. Since $\hat{\psi}$ is the only solution for the equation (4.13), $\hat{\psi}$ is the ML estimate of the parameter ψ. Systematic derivation of the estimators will be the topic of the rest of this chapter.

4.3 Carrier Acquisition

The estimations in carrier acquisition belong to the data-aided (DA) case. The main idea of the DA algorithm is to utilize a preamble ahead of the user data to estimate the parameters. The algorithm for frequency offset and phase offset estimates is operated with preamble samples running at sampling rate $1/T_s$. The phase offset estimator is based on the ML estimation approach and conducted by averaging over the samples in the observation window. The frequency offset estimator is based on the autocorrelation of the samples and weighting the sum of phase differences over consecutive samples. The frequency offset estimation algorithm operates independently of the value of the phase offset. This thesis proposes a new mathematical derivation for the DA frequency estimator, which is presented next.

4.3.1 DA Frequency Offset Estimation

To estimate the frequency offset, we are led to the problem of seeking the maximum of the equivalent likelihood function [8]

$$\Lambda_L(\Omega) = \left| \sum_{i=0}^{N-1} r_i e^{-j\Omega i} \right|^2 = \mathrm{Re}\left\{ \sum_{k=0}^{N-1} \sum_{m=0}^{N-1} r_k r_m^* e^{-j\Omega(k-m)} \right\} \tag{4.14}$$

where Ω is the frequency offset in radians/sample, r_i is the sampled signal, and N is the number of the samples used for frequency offset estimate. Maximizing equation (4.14) with respect to Ω yields the ML estimate of Ω. Taking the derivative of (4.14) with respect to Ω and equating it to zero yields

$$\mathrm{Re}\left\{\sum_{k=0}^{N-1}\sum_{m=0}^{N-1}(-j)(k-m)r_k r_m^* e^{-j\Omega(k-m)}\right\}=0 \tag{4.15}$$

Let $L_F = k-m$ ($k>m$), rearranging terms

$$N_F L_F\ \mathrm{Re}\left\{(-j)R_r(L_F)e^{-j\Omega L_F}\right\}=0 \tag{4.16}$$

where $N_F = N - L_F$ is the number of the time average of samples, and $R_r(L_F)$ denotes the autocorrelation of r_k and is defined as

$$R_r(L_F)\overset{\Delta}{=}\frac{1}{N_F}\sum_{k=L_F}^{L_F+N_F-1} r_k r_{k-L_F}^* \qquad 0<L_F<N-1 \tag{4.17}$$

Equation (4.17) can be explained by the ergodic principle. According to the ergodic principle, if a large number of samples is used, then the random process may be considered ergodic and the autocorrelation of r_k, $R_r(L_F)$, can be approximated by calculating the time average of samples separated by a fixed correlation distance L_F ($0<L_F<N-1$, where $L_F=0$ is of trivial interest) over a window of N_F samples [19]. After some straightforward arithmetic, (4.16) leads to the frequency offset estimate, $\hat{\Omega}$

$$\hat{\Omega}=\frac{1}{L_F}\tan^{-1}\left\{\frac{\mathrm{Im}[R_r(L_F)]}{\mathrm{Re}[R_r(L_F)]}\right\}=\frac{1}{L_F}\tan^{-1}\left\{\frac{\mathrm{Im}\left(\frac{1}{N_F}\sum_{k=L_F}^{L_F+N_F-1} r_k r_{k-L_F}^*\right)}{\mathrm{Re}\left(\frac{1}{N_F}\sum_{k=L_F}^{L_F+N_F-1} r_k r_{k-L_F}^*\right)}\right\} \tag{4.18}$$

To avoid ambiguity, the estimation range of $\hat{\Omega}$ is restricted to $\left|\hat{\Omega}\right| < \pi / L_F$ per sample. The estimation accuracy is dependent on the value of L_F and N_F. If L_F is fixed, then increasing N_F will raise the estimation accuracy. Similarly, if N_F is fixed, the estimation accuracy will be raised as the value of L_F increases, however, the estimation range decreases with increasing L_F. Therefore, the value of L_F must be chosen to obtain a good compromise between estimation accuracy and estimation range. To ensure a valid carrier frequency offset acquisition, the parameter L_F is initially set as small as possible in order to provide the largest acquisition range. Once a frequency acquisition has been established, the residual frequency error can be adjusted in the tracking process. The block diagram of this frequency offset estimator is shown in Figure 4.1.

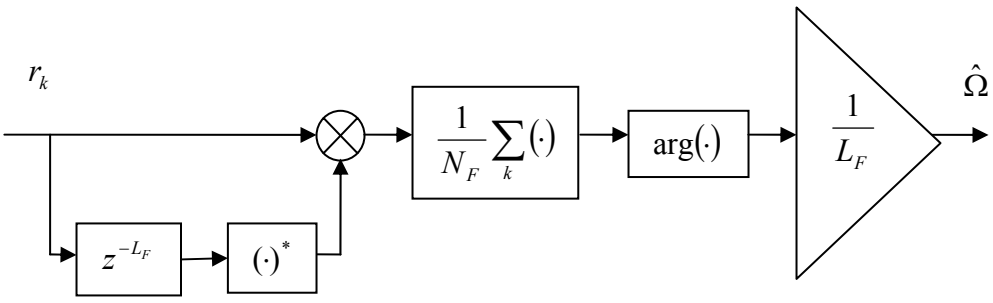

Figure 4.1 Block diagram of DA frequency estimator

Notice from Figure 4.1 that the estimation cannot begin until L_F samples have been stored in memory, therefore requiring a total of $L_F + N_F$ samples. This estimator ideally requires a high sampling rate $1/T_s$, because the larger the number of samples

used for averaging in the observation window, the closer the estimate approaches the true value. This is also the case for the phase estimator to be presented next.

4.3.2 DA Phase Offset Estimation

Assume that we observe a block of N_P frequency-corrected samples in the preamble portion. The k th complex sample can be expressed as

$$\tilde{r}_k = a_k e^{j(\Delta\Omega k+\phi)} + v_k \qquad k = 1,2,...,N_P \quad (4.19)$$

where $\Delta\Omega = \Omega - \hat{\Omega}$ is the residual frequency error carried forward by the inaccurate frequency offset estimate, a_k represents the preamble symbols, and v_k is AWGN with independent in-phase v_k^I and quadrature v_k^Q components, each of zero mean and double-sided PSD of $N_0/2$.

The phase offset estimate, $\hat{\phi}$, is found by seeking the maximum of the likelihood function

$$\Lambda_L(\phi) = \mathrm{Re}\left[\sum_{k=l}^{l+N_P-1} a_k^* \tilde{r}_k e^{-j(\Delta\Omega k+\phi)}\right] \quad (4.20)$$

where the value of l leads to an unbiased estimate and will be explained later. Unfortunately, it is very difficult to derive $\hat{\phi}$ from (4.20) directly. An alternative approach to obtain $\hat{\phi}$ is derived from the first order statistic of the samples

$$E(\tilde{r}_k) = E\left\{a_k e^{j(\Delta\Omega k+\phi)} + v_k^I + jv_k^Q\right\} = E(a_k)\cdot E\left\{e^{j(\Delta\Omega k+\phi)}\right\} = C\cdot E\left\{e^{j(\Delta\Omega k+\phi)}\right\} \quad (4.21)$$

where the noise terms are zero-mean by assumption, and C is a constant resulting from the average of two antipodal preamble symbols. Based on ergodic theory, the mean of $\tilde{r}_k$ can be approximated by its time average. The phase offset estimator is now derived from the time average given by

$$E(\tilde{r}_k) \approx \frac{1}{N_P}\sum_{k=l}^{l+N_P-1}\tilde{r}_k = C\frac{1}{N_P}\sum_{k=l}^{l+N_P-1}e^{j(\Delta\Omega k+\phi)} = \frac{C}{N_P}\frac{\sin(\Delta\Omega N_P/2)}{\sin(\Delta\Omega/2)}e^{j\left[\phi+\Delta\Omega\left(l+\frac{N_P-1}{2}\right)\right]} \quad (4.22)$$

The phase estimate $\hat{\phi}$ is easily found to be the total phase offset estimate at the middle of the observation window of N_P samples, where N_P is odd-valued, by

$$\hat{\phi} = \arg\left(\frac{1}{N_P}\sum_{k=l}^{l+N_P-1}\tilde{r}_k\right) = \phi + \Delta\Omega\cdot\left(l+\frac{N_P-1}{2}\right) \quad (4.23)$$

The estimation range in this case is bounded by $|\hat{\phi}| < \pi$. This phase offset estimator given in (4.23) is very similar to the Viterbi and Viterbi (V&V) algorithm except that M th power of $M = 1$ here for DA operation and the nonlinearity used in V&V can be set to unity [11]. In addition, the sampling rate is higher here than in the V&V technique.

Clearly from (4.23), if the residual frequency error $\Delta\Omega$ is zero, then the estimated phase offset $\hat{\phi}$ corresponds to the fixed phase offset ϕ. However, the estimate $\hat{\phi}$ can not be considered constant in the presence of a frequency error $\Delta\Omega$. A frequency

offset may result in a significant phase estimate variation over the averaging length N_P. In the case of a small residual carrier frequency error, the phase estimate will change linearly with time. Using a one-sided averaging interval will lead to a bias of $\Delta\Omega \cdot k$ with respect to the carrier phase of a sample, which is k samples away from the center, and thus to a degradation of the demodulator performance. By letting $l = -(N_P - 1)/2$ and centering the averaging around the middle sample in the observation window ($-(N_P - 1)/2 \le k \le (N_P - 1)/2$), the odd symmetry of the phase will lead to a cancellation of the linear phase changes, and thus to a unbiased estimate. If we desire a correction of the phase at the end of the preamble, the estimate from the middle must be compensated by the residual frequency error. Thus, it should be carefully considered whether to start tracking from either end of the preamble or whether starting in the middle is the best route. The block diagram of an ML DA phase offset estimator is given in Figure 4.2.

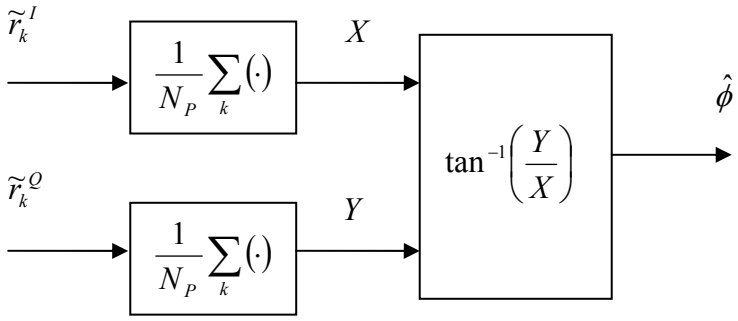

Figure 4.2 Block diagram of DA phase estimator

4.4 Carrier Tracking

The remaining phase error tracking is accomplished by non-data-aided (NDA) estimation as the synchronization parameters are extracted from random user data. The tracking estimation algorithm is different than the acquisition estimation in that it operates at the symbol rate rather than the sample rate, and with the assumption that the symbol timing is known at the receiver. The phase estimator to be described next is in the presence of a very small frequency error. In this technique, the signal is first non-linearly transformed, and then a window of a number of symbols is used to form an estimate of the phase at middle point in the window. The estimate is then used to correct the phase of the symbol. The window slides along for each symbol in the burst. This NDA phase estimation algorithm is based on the V&V phase estimation technique [11] and needs a slight modification for 16-QAM formats.

4.4.1 Overview

The residual frequency error $\Delta\Omega$ in acquisition will result in a significant phase variation over the user data portion. This follows from the fact that the varying phase φ is related to the number of data symbols n as

$$\varphi = \Delta\Omega \cdot k = 2\pi \Delta f \, T_s \cdot k = 2\pi \Delta f \, T \cdot n \tag{4.24}$$

where k is the number of samples, T_s is the sample duration, T is the symbol interval, and Δf is the residual frequency error in Hz. Obviously from (4.24) the phase will change linearly with time. Even though $\Delta fT << 1$, the accrued phase during

the data burst may be several cycles in magnitude because the number of the symbols in the burst $n >> 1$. This increased phase deviation will result in severe errors for detection, especially worse near the end of the burst. Therefore, it is necessary to track the phase variation to reduce and maintain the residual frequency and phase errors within a small tolerable range.

Now that the varying phase φ depends on the number of the symbols in the case of $\Delta fT << 1$, if we divide the user data into some pieces of blocks, the phase variation over one observation window $\varphi = 2\pi \Delta f T \cdot N_W$ may not be significant (N_W is the number of symbols in an observation window). If the received user data portion of the burst is divided into (possibly overlapping) blocks, which are short enough to consider the phase variation to be small over a block, then a single phase estimate can be made for each successive observation window, and correction must be applied before the averaging over the observation window is performed. This is the basic point of the subsequent carrier phase tracking approach.

4.4.2 NDA Carrier Phase Estimation

The following algorithm is based on the idea of the V&V phase estimation technique. In this technique, the signal is first transformed by the nonlinearity and M th power to remove data modulation.

We consider the detection of a sequence of N_W symbols taken from the phase-compensated outputs, one sample per symbol, and its polar form

$$\tilde{\tilde{r}}_n = u_n e^{j(\Delta\Omega n + \Delta\phi)} + v_n = \rho_n e^{j\Phi_n} \qquad n = 1,2,...,N_W \quad (4.25)$$

where n is the symbol index, $\Delta\Omega = 2\pi\Delta fT$ is the frequency error in radians per symbol, $\Delta\phi = \phi - \hat{\phi}$ is phase estimate error, $\rho_n = \sqrt{\left(\tilde{\tilde{r}}_n^I\right)^2 + \left(\tilde{\tilde{r}}_n^Q\right)^2}$ is the magnitude of $\tilde{\tilde{r}}_n$, and $\Phi_n = \tan^{-1}\left(\tilde{\tilde{r}}_n^Q / \tilde{\tilde{r}}_n^I\right)$ is the phase of $\tilde{\tilde{r}}_n$. Then we multiply phase Φ_n by M and perform an arbitrary nonlinear transformation on ρ_n

$$z_n = F(\rho_n)e^{jM\Phi_n} \qquad n = 1,2,...,N_W \quad (4.26)$$

The introduced nonlinearity is described by $F(\rho_n) = (\rho_n)^L$ and $M = 16$ for 16-QAM. Through the above transformation, the 16 constellation phasors are mapped to three phasors (when $L = 0$) or four phasors (when $L \geq 1$) without considering the noise, as shown in Figure 4.3.

If all constellation points are considered equally probable, then the average phase of the phasors in Figure 4.3 (a) or (b) is equal to 0° in an ideal noise-free transmission. The difference in the estimated value from the ideal value 0° is proportional to the average rotation of the constellation points. This situation can be considered to be operationally similar to the DA case and the phase error estimate can be obtained by

$$\hat{\Phi} = \frac{1}{M}\arg\left(\frac{1}{N_W}\sum_{n=-(N_W-1)/2}^{(N_W-1)/2} z_n\right) \quad (4.27)$$

where N_W is odd number. The estimation range is $\left|\hat{\Phi}\right| < \pi/M$.

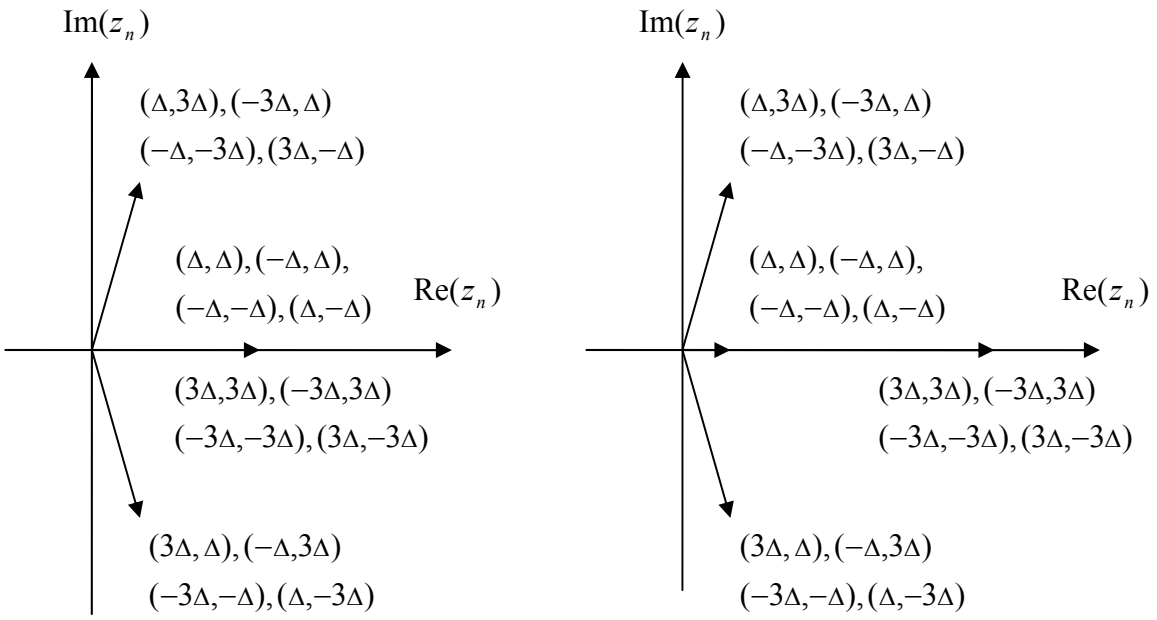

(a) $M = 16 \quad L = 0$ (b) $M = 16 \quad L \geq 1$

Figure 4.3 Nonlinearly transformed 16-QAM constellations

It is shown from equation (4.27) that for $\Delta\Omega \neq 0$, the estimate is unbiased only with respect to the phase of the middle data symbol ($n = 0$) which lies in the observation window ($-(N_W - 1)/2 \leq k \leq (N_W - 1)/2$). Obviously if the observation window N_W is much less than the length of the data burst, all but the first and last $(N_W - 1)/2$ symbol estimates can be made unbiased by overlapping observation windows, that is, by using the preceding and succeeding $(N_W - 1)/2$ symbols to estimate each symbol phase (except for the first and last $(N_W - 1)/2$) individually. The resulting estimates are not independent, since the estimate corresponding to a given observation window takes into account the values of the estimate corresponding to previous observation window, but they are unbiased. The disadvantage is that this

requires approximately N_W as many operations as performing a single estimate for all N_W symbols in the observation window. The block diagram of the ML NDA carrier phase tracker is given in Figure 4.4.

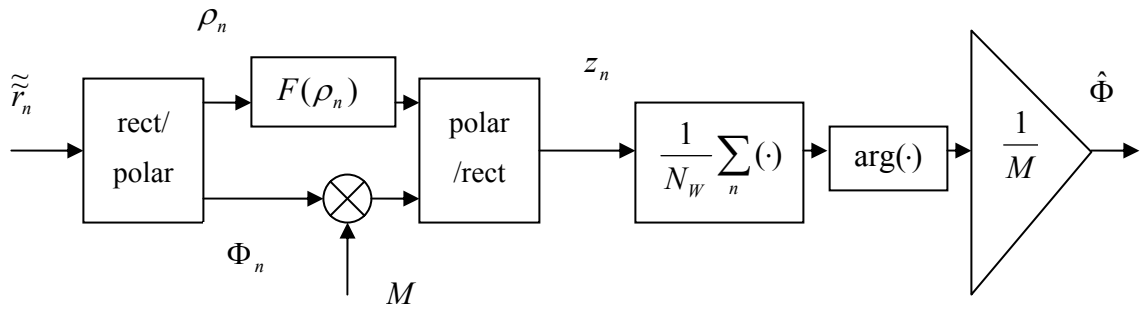

Figure 4.4 Block diagram of NDA carrier phase tracker

It is shown in Figure 4.4 that for each symbol, we perform a rectangular-to-polar transformation first, then multiply the phase of $\tilde{\tilde{r}}_n$ by M ($M = 16$), which in effect removes the data dependency of the 16-QAM modulation, then perform an arbitrary nonlinear transformation on the magnitude of $\tilde{\tilde{r}}_n$; and finally perform a polar-to-rectangular transformation on the result. The rest of the algorithm is similar to the carrier phase estimator in acquisition. Although this phase tracker is similar to the phase estimator in acquisition, it turns out to have a drawback of excessively increasing noise levels because of the M th power operation.

4.4.3 Window Size Selection

The phase estimate $\hat{\Phi}$ resulting from equation (4.27) is unbiased with respect to the phase at the center of a single observation window and may be represented as

$$\hat{\Phi} = \Delta\phi + \theta + \varepsilon \tag{4.28}$$

where $\Delta\phi$ is the phase error delivered from inaccurate frequency and phase estimates in acquisition, θ is the phase error introduced by the average of unsymmetrical 16-QAM symbols, and ε is additive Gaussian noise phase. In the presence of a small residual frequency error $\Delta\Omega$, the values of θ and ε, and the estimation error variance after averaging the M th power nonlinearity output samples over the observation window are decreasing with increasing N_W. Because the average value of a large number of symbols is close to its statistical mean for random variables based on ergodic theory. As a result, the noise phase ε is zero by definition and θ is also close to zero as 16 symbols are equally probable. The optimum value of N_W which minimizes the estimation error variance for a given $\Delta\Omega$ must exist, and can be optimized to yield minimum estimate error and minimum associated BER degradation [4]. Carefully choosing the window size is directly related to the BER performance of the estimator. It will be discussed in the next chapter.

4.5 Summary

This chapter presented the ML-based feedforward carrier acquisition and carrier tracking techniques for 16-QAM signals in the AWGN environment. The received signal model is given in the very beginning of this chapter, then ML parameter estimation technique is introduced as a theory base for the following estimators presented.

In acquisition, the carrier phase and frequency offsets are estimated with the help of preamble (data-aided), and the algorithms were based on oversampling of the received data sequence, whereas the estimates in tracking mode make use of symbol timing estimate and the algorithm borrows the idea of the V&V NDA phase estimation technique. The estimation operates at very small frequency error. In this technique, the packet is buffered for a window of number of symbols, and then these symbols are used to determine a phase estimate by using nonlinear power-of-M techniques to get rid of the offsets of data modulation. The observation window size can be optimized to yield minimum estimate error and minimum associated BER degradation. The performance of the estimators developed will be discussed in Chapter 5.

Chapter 5

SIMULATION RESULTS AND PERFORMANCE EVALUATION OF CARRIER RECOVERY SYSTEM

This chapter focuses on analyzing the estimation algorithms for the carrier recovery system developed in Chapter 4. The estimators' performance is simulated and evaluated for 16-QAM systems. The estimate bias and variance as well as BER are used as the measures to evaluate the performance characteristics of the estimators. The BER performance of the estimators in the presence of some impairments (frequency offset, phase offset, and AWGN) is evaluated and compared.

5.1 Performance Measurement of Estimators

Before evaluating the carrier recovery system, we first restrict our attention to the tools used to measure the system performance.

5.1.1 Estimation Error Measurement

The quality of a signal parameter estimate can be assessed in terms of estimate bias and the variance of the estimation error. The bias of an estimate, say $\hat{\psi}$, is defined as [16].

$$\text{bias} = \left| E(\hat{\psi}) - \psi \right| \tag{5.1}$$

where ψ is the true value of the unknown parameter. When $E(\hat{\psi}) = \psi$, we say that the estimate is *unbiased*. The estimation error equals the difference between the true value ψ and the estimate $\hat{\psi}$, i.e. $\Delta\psi = \psi - \hat{\psi}$. The variance of the estimation error is defined as [3].

$$\sigma^2 = \text{var}(\psi - \hat{\psi}) = E\left\{ \left[\hat{\psi} - E(\hat{\psi}) \right]^2 \right\} \tag{5.2}$$

This variance provides a measure of the spread of error. A good estimate is one that has both a small bias and a small variance.

5.1.2 BER Measurement

It is often convenient to specify system performance by the *bit error rate* (BER) in practice. BER can be defined as the number of bits received that exhibit errors divided by the number of bits sent.

$$\text{BER} = \left. \frac{number \quad of \quad bits \quad in \quad error}{total \quad number \quad of \quad bits \quad transmitted} \right|_{\text{relatively long time}} \tag{5.3}$$

The BER must be measured over a "relatively long time" to ensure the ratio represents a statistically significant probability. That means by sending a large number of bits, a more accurate BER performance of the system under evaluation will be acquired. This often presents a practical measurement difficulty when measuring low BER due to the large amount of data that must be transmitted. The BER measurement for a communication system can be implemented by the well-known Monte Carlo simulation methodology [20], as shown in Figure 5.1.

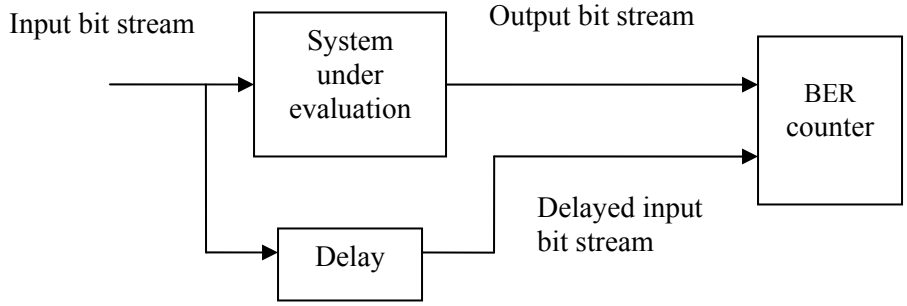

Figure 5.1 Block diagram of Monte Carlo simulation methodology

In the Monte Carlo simulation method, an input bit stream is fed to the system under evaluation. The output bit stream, which contains the combined effects of the impairments, is compared to the input bit stream in the BER counter which computes the BER by counting the number of discrepancies between the input and output bits. Note that the input bit stream must be delayed by an amount equivalent to the delay introduced by the system under evaluation before entering the BER meter.

5.1.3 BER Degradation due to Synchronization Errors

The BER performance of 16-QAM systems under the assumption of a perfect synchronization has been well treated in Section 2.5.1. In practice, however, the synchronizer provides an estimate which most of the time exhibits small fluctuations about the true value (estimation errors). If we would rather study the influence of the parameter estimation errors on the detection process, these fluctuations will give rise to a BER degradation as compared to perfect synchronization and reduce the performance. The degradation with respect to perfect synchronization caused by the variance of the synchronization parameter estimates can be called *detection loss* [4]. It is important to know this BER degradation in terms of the accuracy of the estimates provided by the synchronizer, so that the synchronizer can be designed to yield a target BER degradation (which should not exceed about 1dB for most applications). One of the most important metrics of performance in digital communication system is a plot of BER versus E_b/N_0 , as shown in Figure 5.2.

The solid-line curve in Figure 5.2 shows the ideal BER for a Gray-coded 16-QAM system with perfect synchronization and infinite precision arithmetic while the dotted line shows the simulation results of a representative degraded performance characteristic caused by imperfect carrier synchronization. It is seen that the degraded performance curve is indeed approximately obtained by shifting the perfect system performance curve by D dB to the right. The magnitude of D is the increase of the E_b/N_0 required to compensate for the degradation caused by synchronization errors

with respect to a receiver with perfect synchronization. In the following we determine the BER degradation caused by random synchronization errors.

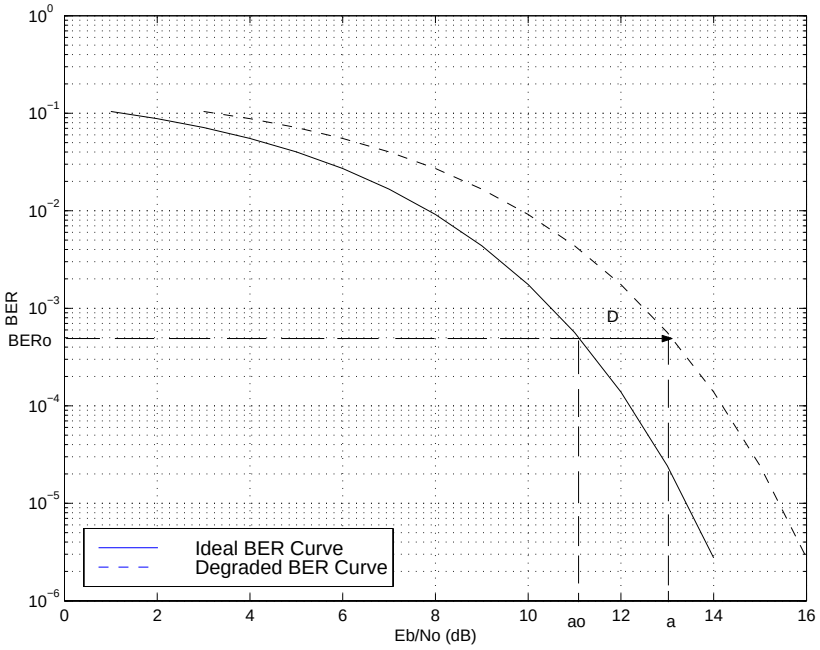

Figure 5.2 BER degradation (in dB) due to imperfect synchronization

Let the notation of e represents the synchronization error: $e = \Delta\Omega = \Omega - \hat{\Omega}$ in the case of a carrier frequency error, whereas $e = \Delta\phi = \phi - \hat{\phi}$ in the case of a carrier phase error. The BER degradation D (detection loss), measured in decibels (dB), is defined as the increase of E_b/N_0, required to maintain the same BER as the receiver without synchronization errors. Hence, the BER degradation D at a BER value of BER_0 is given by

$$D = 10\log_{10}(\alpha/\alpha_0) \tag{5.4}$$

where α and α_0 are signal-to-noise ratio per bit (reference to Section 2.5.1) for a particular BER and determined by

$$\text{BER}_0 \approx P(0;\alpha_0) = E_e\left[P(e;\alpha)\right] \tag{5.5}$$

In (5.5), $P(0;\alpha_0)$ denotes the ideal BER given $E_b/N_0 = \alpha_0$, $P(e;\alpha)$ represents the experimental BER, corresponding to a synchronization error e, at $E_b/N_0 = \alpha$, and $E_e[\cdot]$ denotes averaging over the random synchronization error e. $E_e\left[P(e;\alpha)\right]$ can be obtained by iterating the simulation for some specified number of iterations and computing the average of BER's obtained in these iterations. The experimental BER curve is acquired by repeating for the entire simulation over all the receiver operating points of interest. The larger the number of trials, the closer the results are to $E_e\left[P(e;\alpha)\right]$.

To evaluate the BER performance of the synchronization system in the burst-mode environment which is the case for this thesis, two situations need being considered. For a synchronizer operating in long burst mode, only several burst packets being sent may be statistical sufficient for calculating BER. More burst packets need to be sent for a synchronizer operating in short burst mode however, to achieve statistical description of BER. Since this iteration method can be quite time consuming, the number of simulation trials should be a reasonable compromise between simulation run time and simulation result accuracy.

In fact, the BER measuring method is consistent with the estimation error measuring method. For a small estimate variance, the BER degradation caused by synchronization errors is basically proportional to the estimate variance. Both measuring methods are used to evaluate the performance of the estimators in this thesis to provide different information.

5.2 Simulation Issues

As simulation is used to imitate the behaviour of the actual hardware found in communication systems, it is the best way to make the algorithm designer aware of the strong interaction between algorithm and architecture design. The simulations in this thesis were carried out using Matlab software. The whole 16-QAM communication system and the burst packets are set up and generated by using Matlab functions. The corresponding Matlab code can be found in Appendix A.

The main objective of this simulation is to evaluate the proposed synchronization algorithms for the carrier recovery system of the 16-QAM signal. To demonstrate the application validity of the proposed algorithms, specifications similar to the IEEE 802.16 standard for wireless Metropolitan Area Networks (MAN) are used to analyze the 16-QAM carrier recovery system. The radio frequency (RF) band is chosen to be 10 GHz. The target data transmission rate is 80 Mbps, corresponding to a symbol rate of 20 Msps for 16-QAM systems.

5.2.1 Baseband Simulation

Since the carrier is a high frequency signal, modeling bandpass communication systems involves high computational loads. To alleviate this problem, *baseband simulation models* are employed throughout this research, and all the signals are modeled as baseband equivalent representation. All the signals are complex and should be interpreted as complex envelopes of real RF signals.

In fact, the bandpass model of the detection process is virtually identical to the baseband model. That is because a received bandpass waveform is first transformed to a baseband waveform before the final detection step takes place. For linear systems, the mathematics of the detection is unaffected by a shift in frequency. All linear signal-processing simulations can take place at baseband with the same results as at bandpass. This means that the performance of most digital communication systems will often be described and analyzed as if the transmission channel is a baseband channel [2].

The problem is simplified with this identity. For example, let B be the bandwidth of the information signal. The baseband simulation only requires the simulation sampling rate to be larger than $2B$ in order to accommodate the bandwidth of the baseband information signal. This is far less than would be required with the bandpass representation.

5.2.2 Simulation Setup

The simulation is set up by using the Monte Carlo simulation technique. The detailed setup block diagram of a 16-QAM baseband communication system is illustrated in Figure 5.3.

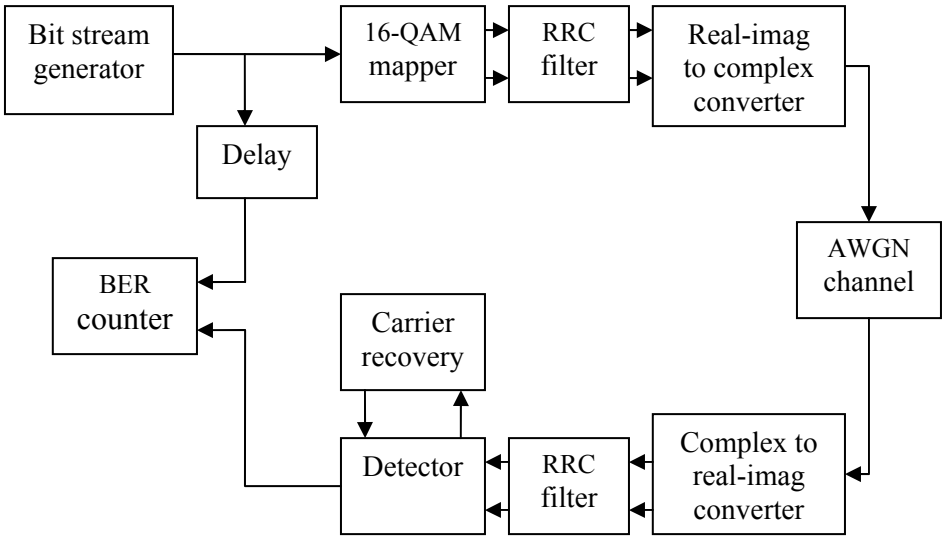

Figure 5.3 Block diagram of simulation setup for a 16-QAM baseband system

This simulation test setup is done much in the similar way as a practical system would be tested. Various system parameters may be changed to set up specific conditions for testing. The bit stream generator generates a number of burst packets. The length of the burst can be long or short according to the requirement. Synchronization occurs at the start of each individual burst and is carried out independently from one burst to the next. As the synchronization has no memory from burst to burst in this testing, "resynchronization" is performed on a burst-by-burst basis. The same synchronization parameters (including initial carrier frequency offset

and phase offset) are used for all data detected. BER is only calculated on the data portion of the packets (not the preamble portion) to evaluate the system performance.

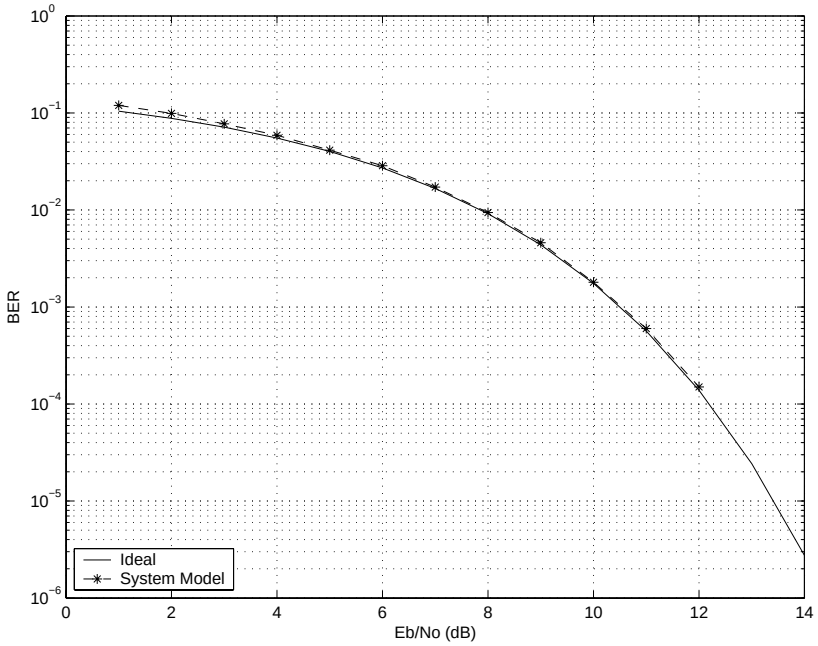

Figure 5.4 BER performance of 16-QAM system model under ideal environment

The BER performance of this system in an "ideal" burst-mode environment for 16-QAM is shown in Figure 5.4. "Ideal" means the system has perfect carrier recovery, a Nyquist response, and zero ISI, and is only corrupted by AWGN. The burst packet of 2000 user data symbols is used and a total of 25 burst packets are sent in the simulation. The simulation result shows that the performance of this system model agrees closely to the ideal BER curve, indicating that the whole system is well designed and modeled, and gives confidence in the validity of the simulation platform. The various simulation subsystems are explained below:

Bit Stream Generator

The bit stream generator generates burst packets in terms of binary numbers, which include a known sequence (preamble) and a random data sequence (user data).

16-QAM Mapper

This block maps the input bit stream into complex symbols according to the 16-QAM constellation. As a result, a repeating sequence of 16-QAM symbols 0010 - 0110 (reference to Figure 2.2), which are two points on opposite sides of I channel, is used as the preamble sequence in the simulation.

Transmit and Receive Filters

The transmit RRC filter converts symbols to baseband waveforms to be transmitted over the channel. This filter is combined with the matched RRC filter in the receiver to meet Nyquist's criterion for zero ISI. The combined result of the RRC filters should be a RC filter. Figure 5.5 shows the relationship between the original inphase component of 16-QAM signal and the filtered output of the inphase component, and also compares the inphase signal output filtered by a normal RC filter and two combined RRC filters designed in the simulation. As can be seen in Figure 5.5, applying two RRC filter results the same filtered signal as that of using a normal RC filter. The roll-off factor of each RRC filter and RC filter is chosen to be 0.5 in the simulation.

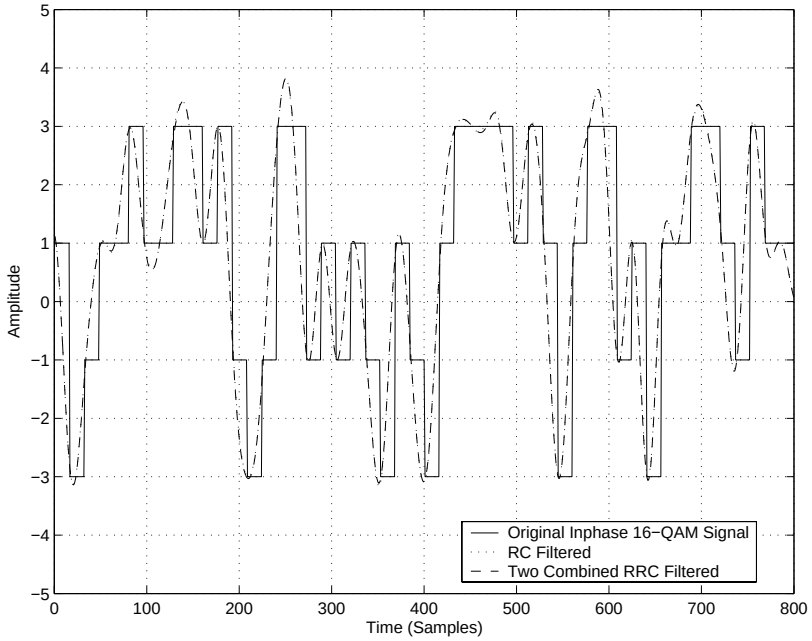

Figure 5.5 Comparison of a RC and two combined RRC filtered inphase component of 16-QAM signal

AWGN Channel

This block adds AWGN with a specified variance to the transmitted signal. The AWGN is modeled as the combination of two independent and normally distributed I and Q components of random noise v, each of zero mean and $N_0/2$ PSD. The reason of doing this is to prevent correlation between the I and Q noise components. Since the mean of the AWGN noise is zero ($m_v = 0$), the variance of the noise equals to

$$\sigma_v^2 = E(v^2) - [E(v)]^2 = R_v(0) - m_v = \frac{N_0}{2} \tag{5.6}$$

where the autocorrelation function for broadband white noise is $R_v(n) = \frac{N_0}{2}\delta(n)$.

Assuming that the symbol points in the 16-QAM constellation are equally probable, the average transmitted energy per symbol can be calculated by [16]

$$E_s = \frac{1}{M}\sum_{m=1}^{M}\left[\left(A_m^I\right)^2 + \left(A_m^Q\right)^2\right] \tag{5.7}$$

where $A_m^I, A_m^Q \in \left\{\pm 1\Delta, \pm 3\Delta, ..., \pm(\sqrt{M}-1)\Delta\right\}$ are referred to the I and Q amplitudes corresponding to the M possible symbols in the 16-QAM constellation (where $M = 16$). The relationship between the average SNR per symbol E_s/N_0 and the average SNR per bit E_b/N_0 is [2]

$$\frac{E_s}{N_0} = \frac{E_b}{N_0}\log_2 M \tag{5.8}$$

Therefore, the noise variance is represented as

$$\sigma_v^2 = \frac{1}{2}\cdot\frac{E_s}{\left(\log_2 M\right)E_b/N_0} \tag{5.9}$$

As a result, the AWGN can be modeled in terms of its mean and variance in Matlab®. Usually, E_b/N_0 is characterized in dB.

Detector

The detector decides what possible symbols were transmitted. The detector computes the Euclidean distance between the received noise-corrupted symbol point

and the M possible transmitted points, and selects the symbol closest to the received point.

Carrier Recovery System

The carrier recovery system is the major part under evaluation in this thesis. The simulation is carried out using a sampling rate R_s of 16 times the symbol rate R (i.e., $k = R_s / R = 16$). The frequency offset f (in Hertz) can be obtained from $\Omega = 2\pi f (T/k)$, where Ω (in radians per sample) is the frequency offset normalized to sampling rate and T (in seconds) is the symbol duration, and is given as a percentage of the symbol rate R in the subsequent system evaluation. Table 5.1 shows f associated with a number of Ω used in the simulation.

Table 5.1 The conversion between f and Ω

f $(\%R)$	Ω (radians/sample)	Ω $(^\circ/\text{sample})$	Ω $(^\circ/\text{symbol})$
2.16e-03	8.48e-06	4.86e-04	7.78e-03
3.14e-03	1.23e-05	7.07e-04	1.13e-02
4.98e-03	1.96e-05	1.12e-03	1.79e-02
8.19e-03	3.22e-05	1.84e-03	2.95e-02
1.00e-01	3.93e-04	2.25e-02	3.60e-01
2.00e-01	7.85e-04	4.50e-02	7.20e-01
6.00e-01	2.36e-03	1.35e-01	2.16e+00
9.00e-01	3.53e-03	2.03e-01	3.24e+00

For a 16-QAM communication system operating at IEEE 802.16 standard as mentioned earlier, the translated frequency offset caused by 1 ppm instability of a crystal oscillator would be ± 10 kHz, or a maximum frequency offset between the transmitter and receiver of 20 kHz. This frequency offset produces phase rotation in terms of symbols as $3.60e-01^{\circ}/\text{symbol}$ or $1.00e-01\%R$ in terms of symbol rate R. This frequency offset will be used as the initial frequency offset to evaluate the carrier recovery system next.

5.3 Performance Evaluation of Carrier Recovery System

5.3.1 DA Frequency Estimator

The performance of the proposed DA frequency estimator in carrier acquisition will be evaluated in this section. Figure 5.6 plots the mean of the frequency offset estimate $\hat{f}$, which is defined as $\bar{\hat{f}} = \frac{1}{N}\sum_{n=1}^{N}\hat{f}(n)$ and obtained by the average of $N = 10000$ trials at $E_b/N_0 = 10\,\text{dB}$ (The values of trial times and E_b/N_0 is the same in the following simulations without being specified.). The correlation distance L_F and the number of averaging samples N_F are set to $L_F = 800$ samples (50 symbols) and $N_F = 816$ samples (51 symbols), and a total of 101 preamble symbols is needed. Indeed, the estimator assesses on the average of the frequency offset for about 97% of the range of $\left[-\frac{100k}{2L_F}\%R \quad \frac{100k}{2L_F}\%R\right]$, outside which it suffers from modulus 2π

fold-over. The phase offset can be any value in $[-\pi, \pi]$ and does not impact the frequency offset estimation, which is determined by the estimation algorithm.

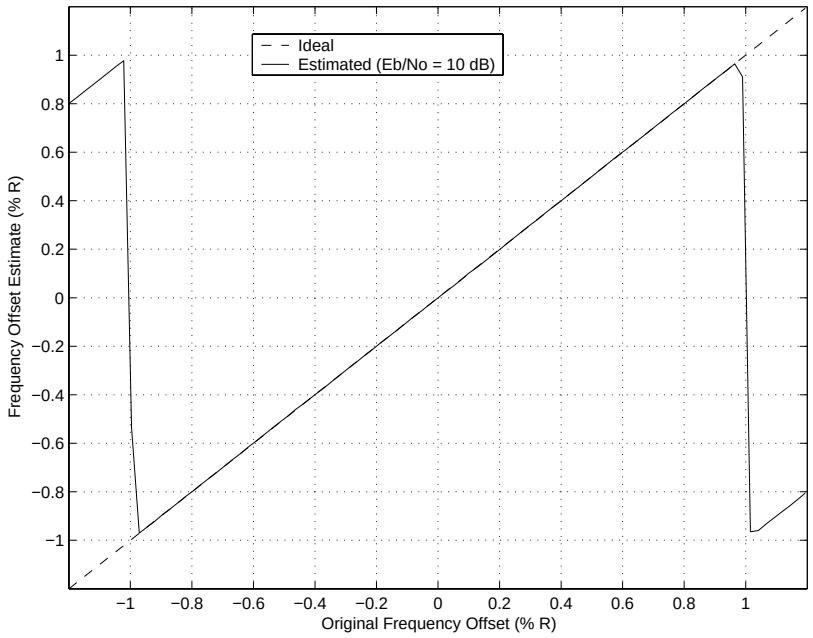

Figure 5.6 Mean of $\hat{f}$ versus true frequency offset when $L_F = 800$ samples

The accuracy of the frequency estimation is dependent on the parameters of L_F and N_F. The simulation will show next how L_F and N_F affect the frequency estimation respectively in terms of the estimate bias which is defined as $\left|\bar{\hat{f}} - f\right|$ and variance which is defined as $\sigma^2 = \frac{1}{N}\sum_{n=1}^{N}\left[\hat{f}(n) - \bar{\hat{f}}\right]^2$. The initial frequency offset is set at $f = 1.00e-01\%R$ in the simulation. Table 5.2 compares the estimate bias and variance in the case of $L_F = 50$ symbols and $L_F = 70$ symbols respectively, with the same averaging window $N_F = 51$ symbols. This table shows that increasing L_F reduces both estimate bias and variance.

Table 5.2 Statistics of the frequency estimate for different L_F

Total preamble (symbols)	Estimate bias $(\%R)$	Estimate variance $(\%R)$
101 ($L_F = 50$, $N_F = 51$)	9.42e-04	5.26e-05
121 ($L_F = 70$, $N_F = 51$)	6.29e-04	2.64e-05

On the other hand, the estimation range is decreased if increasing L_F, as shown in Figure 5.7 where $L_F = 1120$ samples (70 symbols) compared to Figure 5.6 where $L_F = 800$ samples (50 symbols). The estimate range decreases from $[-0.97\%R,\ \ 0.97\%R]$ to $[-0.69\%R,\ \ 0.69\%R]$. Therefore, the value of L_F must be chosen to obtain a good compromise between estimation accuracy and estimation range.

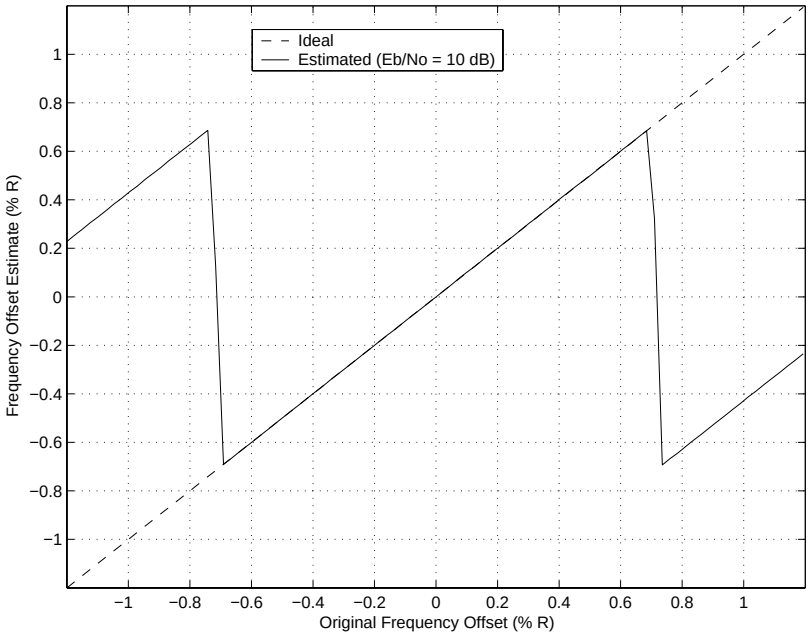

Figure 5.7 Mean of $\hat{f}$ versus true frequency offset when $L_F = 1120$ samples

We should be also aware that, theoretically, if the correlation distance is set to $L_F = 1$ sample for the proposed frequency estimator, the estimation range of $\hat{f}$ should be over $[-800\%R, \quad 800\%R]$ (as explained in Section 4.3.1). However, the frequency estimation range is much smaller in the practical system because the frequency components of the received signal are out of the band of the matched filter. It can be seen in Figure 5.8 that, for the case of $L_F = 1$ sample and $N_F = 1615$ samples (a total of 101 preamble symbols), the maximum estimation range that this carrier recovery system can reach is only approximately $[-50\%R, \quad 50\%R]$, beyond this range the estimation is no longer valid.

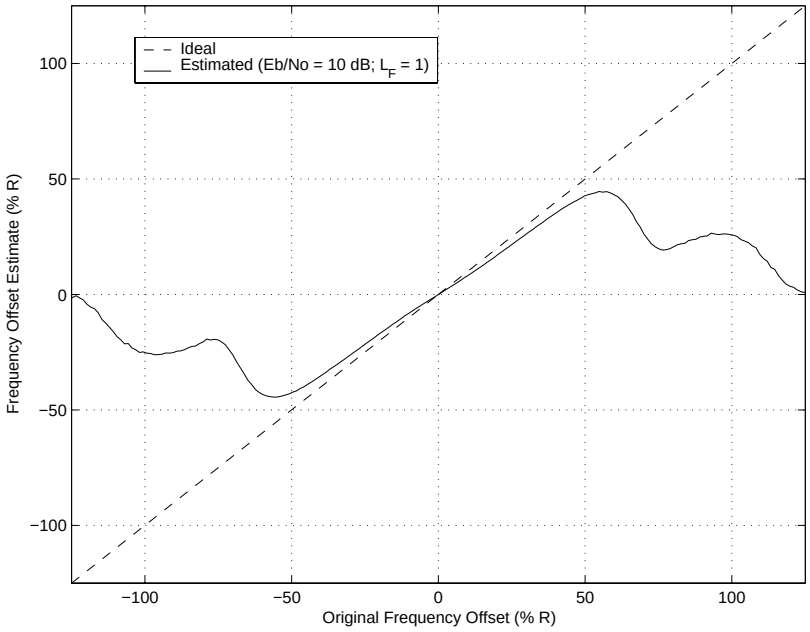

Figure 5.8 Mean of $\hat{f}$ versus true frequency offset when $L_F = 1$ sample

Also notice that $\hat{f}$ is significantly biased even within this range. This is because the value of L_F is not optimum. If setting $L_F = 16$ samples and the other parameters stay the same as above, the result turns out much better as shown in Figure 5.9.

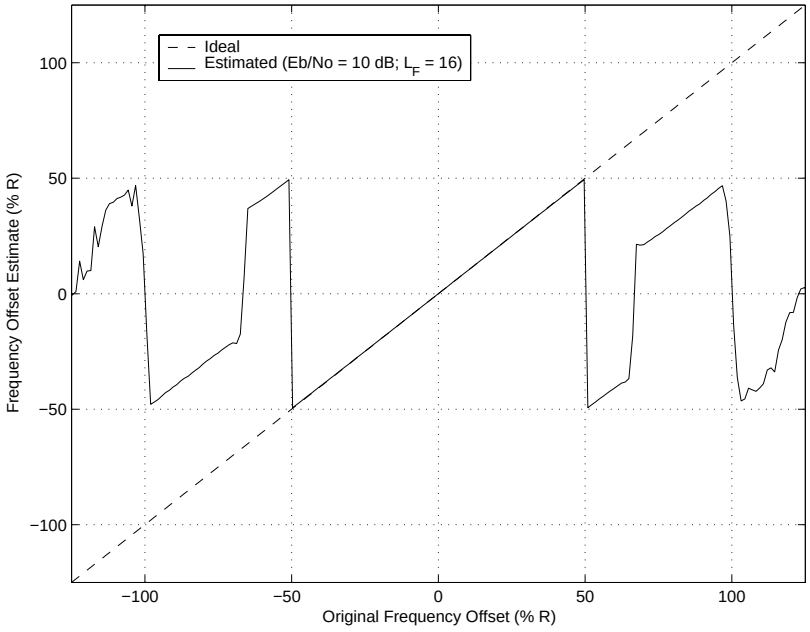

Figure 5.9 Mean of $\hat{f}$ versus true frequency offset when $L_F = 16$ samples

Now let us look at how the averaging window N_F affects the frequency estimation. Table 5.3 gives the estimate bias and variance in the case of $N_F = 51$ symbols and $N_F = 71$ symbols with the same $L_F = 50$ symbols. The table shows that both estimate bias and variance are reduced if N_F is increased.

Table 5.3 Statistics of the frequency estimate for different N_F

Total preamble (symbols)	Estimate bias $(\%R)$	Estimate variance $(\%R)$
101 ($N_F = 51,\ L_F = 50$)	9.42e-04	5.26e-05
121 ($N_F = 71,\ L_F = 50$)	6.42e-04	2.74e-05

We can conclude that the estimation accuracy is improved if either L_F or N_F is increased. For the better performance, increasing L_F rather than N_F is preferable in hardware implementation since L_F only requires additional memory, whereas N_F increases computational complexity. Generally speaking, the accuracy of DA frequency estimation is strongly dependent on the length of the preamble (which is the sum of L_F and N_F). The statistics of the frequency estimation for different preamble length is given in Table 5.4. It can be seen that the estimation is improved using longer preamble.

Table 5.4 Statistics of the frequency estimate for different preamble length

E_b/N_0 (dB)	Total preamble (symbols)	Estimate bias ($\%R$)	Standard deviation ($\%R$)	Max $\lvert\Delta f\rvert$ ($\%R$)
10	81	1.43e-03	1.01e-02	4.42e-02
	101	9.42e-04	7.25e-03	2.89e-02
	121	4.59e-04	5.45e-03	2.43e-02
15	81	1.39e-03	5.66e-03	2.38e-02
	101	8.74e-04	4.11e-03	1.82e-02
	121	5.95e-04	3.07e-03	1.17e-02
20	81	1.40e-03	3.19e-03	1.32e-02
	101	8.51e-04	2.29e-03	9.63e-03
	121	5.85e-04	1.75e-03	7.41e-03
25	81	1.36e-03	1.86e-03	9.23e-03
	101	8.52e-04	1.31e-03	6.15e-03
	121	6.02e-04	1.00e-03	4.19e-03

The effect of the preamble length on the BER performance of the frequency estimator is shown in Figure 5.10. Only 10 symbols are used in the user data portion in

order to keep the effect of the residual frequency error Δf as small as possible. A total of 500 burst packets are sent in order to make BER statistically significant.

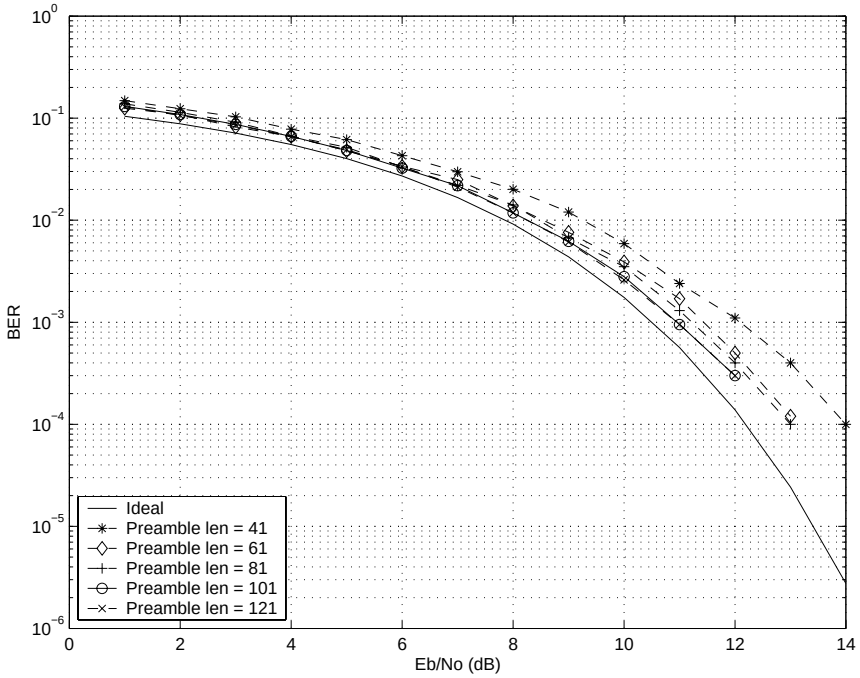

Figure 5.10 BER performance of frequency estimator for different preamble lengths

Figure 5.10 also shows that the BER performance of the estimator is improved as the preamble length increases. The preamble length should be carefully selected so that the range of the residual frequency error can be tolerated by the carrier tracker and also be efficient for burst-mode transmission. Since the preamble of 101 symbols gives an acceptable BER performance (about 0.4 dB loss at a BER of 10^{-3}), it is used to evaluate the estimators' performance in this thesis.

It is worth to mention here that when the frequency offset is small, the variation of the carrier phase over an interval equal to the effective duration of the baseband pulse $g(t)$, which equals a few symbol intervals, is negligible. However, when the initial

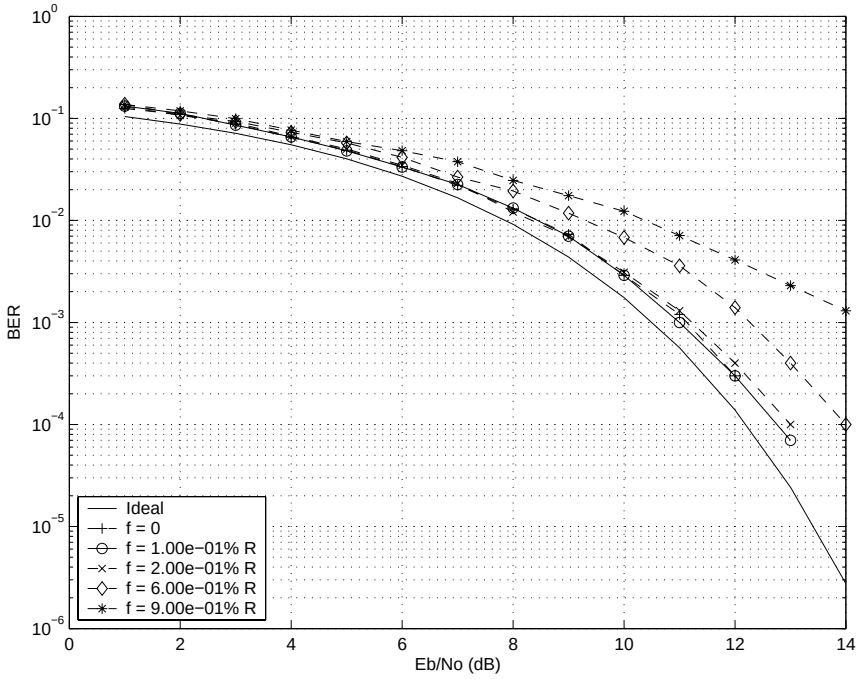

Figure 5.11 BER performance of frequency estimator for different f

frequency offset is large, the received signal will be ill-centered with respect to the matched filter. This gives rise to a distorted matched filter output pulse (as compared to the case $f = 0$), which introduces ISI [3]. The ISI at the output of the receiver matched filter is likely to cause an unacceptable degradation of the receiver performance because filtered samples will not be ISI free. Using these samples to estimate the carrier offsets might produce a biased estimate and degrade the performance of the estimators, as shown in Figure 5.11 (where total 500 burst packets are sent, each has 101 preamble symbols and 10 user data symbols). This ISI problem might be solved in practice by adding a pre-stage frequency estimator to lower the frequency offset to be estimated [3]. Although this coarse estimate may still substantially deviate from the true value, the quality of this first estimate would guarantee that the frequency offset is within an acceptable range for ISI before the

frequency-adjusted samples are fed to the digital matched filter. Figure 5.11 gives convincing result that the frequency offset of $f = 1.00e-01\%R$ is small enough for ISI to be neglected and can be chosen to evaluate the estimators in this thesis.

The residual frequency error (even if it is very small) cannot be neglected in the case of long burst operation. For example, if the residual frequency error is chosen to be $\Delta f = 3.14e-03\%R$ (see Table 5.4), the BER comparison of the estimator in short burst (where the user data packet has 300 symbols and 100 burst packets are sent) and in long burst (where the user data packet has 2000 symbols) is shown in Figure 5.12.

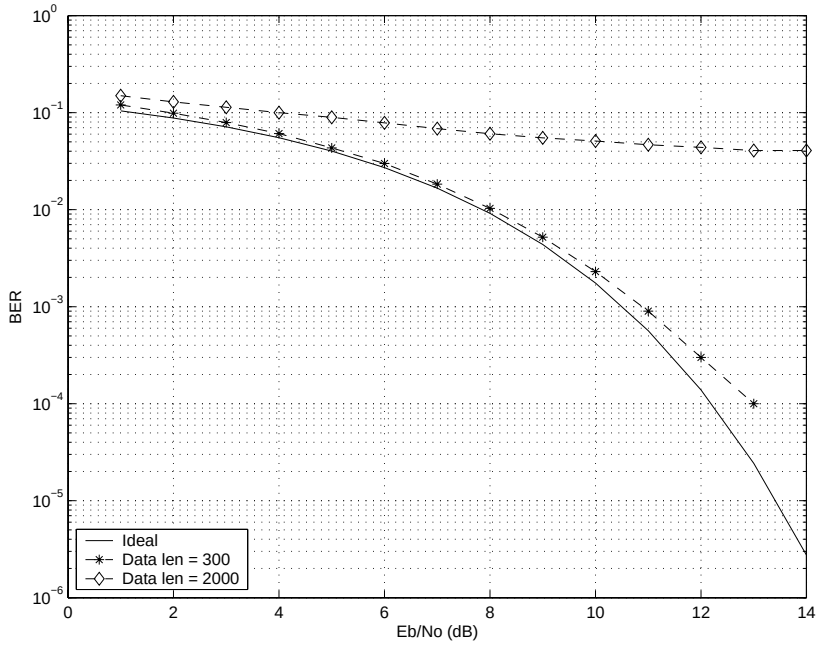

Figure 5.12 BER performance of frequency estimator for short and long burst

Obviously, for long burst operation, the BER performance of the estimator is significantly degraded by the residual frequency error, indicating that a single frequency estimate per burst is no longer sufficient. In this case, additional successive

estimates are required to track the fluctuation of the frequency error with time. The tracking for the long burst will be explained in Section 5.3.3.

5.3.2 DA Phase Estimator

This section presents performance evaluation for the DA phase estimator in the carrier acquisition. Figure 5.13 graphs the mean of phase offset estimate versus the true phase offset for the case of zero frequency error ($\Delta f = 0$) and 10 preamble symbols (160 samples). The purpose of setting $\Delta f = 0$ is to remove the additional complication so that the "pure" phase estimation algorithm could more objectively be assessed. From the figure, the estimator assesses on the average of the phase offset for about 96% of the entire range $[-\pi, \pi]$ except where the phase folds over owing to the

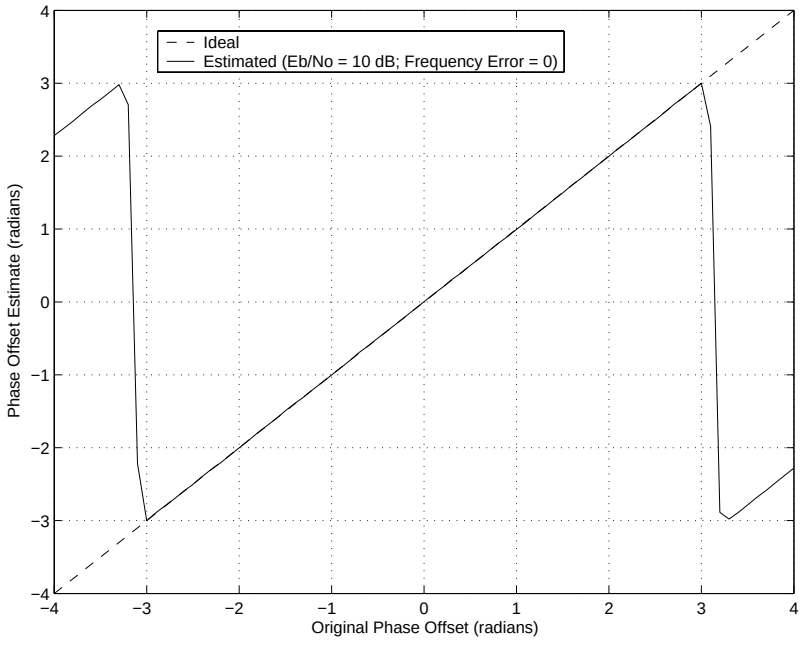

Figure 5.13 Mean of $\hat{\phi}$ versus true phase offset

modulus 2π property of $\hat{\phi}$. The statistics of the phase estimation for different preamble length are shown in Table 5.5. The initial phase offset is set at $\phi = 45^\circ$ and the frequency error is zero. It is seen that the estimation is improved as the preamble length increases.

Table 5.5 Statistics of the phase estimate for different preamble length

E_b/N_0 (dB)	Total preamble (symbols)	Estimate bias ($^\circ$)	Standard deviation ($^\circ$)	Maximum $\lvert\Delta\phi\rvert$ ($^\circ$)
10	10	9.38e-01	2.22e+00	1.02e+01
	20	5.98e-01	1.53e+00	6.48e+00
	30	3.94e-01	1.26e+00	5.42e+00
15	10	9.60e-01	1.25e+00	5.79e+00
	20	6.16e-01	8.81e-01	3.89e+00
	30	4.20e-01	7.17e-01	3.05e+00
20	10	9.68e-01	6.93e-01	4.17e+00
	20	6.21e-01	5.18e-01	2.29e+00
	30	4.15e-01	4.13e-01	2.00e+00
25	10	1.26e+00	5.14e-01	3.05e+00
	20	6.20e-01	3.19e-01	1.78e+00
	30	4.10e-01	2.49e-01	1.32e+00

The BER performance of the phase estimator for different preamble length is shown in Figure 5.14. The initial phase offset is set at $\phi = 45^\circ$ and the frequency error is zero. The user data portion has 2000 symbols and total 20 burst packets are used. It is observed in Figure 5.14 that the performance of the DA phase estimator is mildly dependent on the length of the preamble. With only 10 preamble symbols, the

detection loss is only about 0.3dB at BER of 10^{-3}, indicating that the carrier phase offset estimation is quickly and accurately identified.

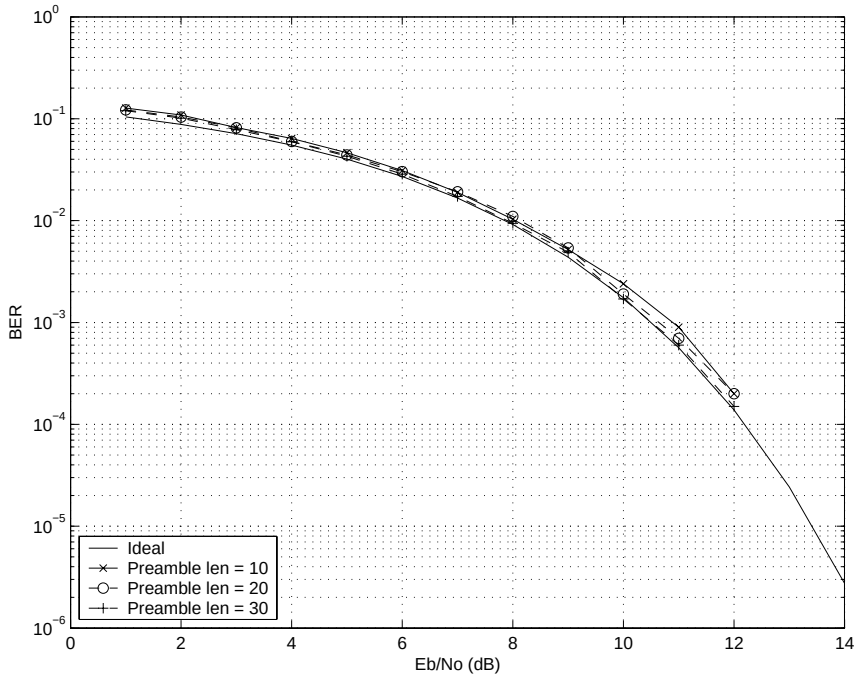

Figure 5.14 BER performance of the phase estimator for different preamble lengths

The phase offset estimate is an estimate of the phase of a sample in the exact middle of the preamble. If we desire a phase correction at the end of the preamble, the estimate from the middle must be compensated by the inaccurate frequency estimate delivered from the previous frequency estimation stage. Due to frequency estimation delivering very small residual frequency offset (the statistical residual frequency error $\Delta f < 3.14e-03\%R$ at $E_b/N_0 = 20\,\text{dB}$ in Table 5.4), and very short preamble (only 10 symbols) needed for phase offset estimation, the phase variation over the estimation period due to Δf is considered insignificant. In this case, the phase correction can be made at the end of the preamble.

5.3.3 NDA Phase Tracker

The BER performance comparison of long burst operation with and without tracking is shown in Figure 5.15. The initial phase offset is $\phi = 45^\circ$ and the residual frequency error is still set to $\Delta f = 3.14e-03\%R$. Each burst includes 111 preamble symbols (101-symbol for the frequency estimation and 10-symbol for the phase estimation) and 2000 user data symbols, and total 100 bursts are sent. These parameters are used to evaluate the NDA phase tracker in this section.

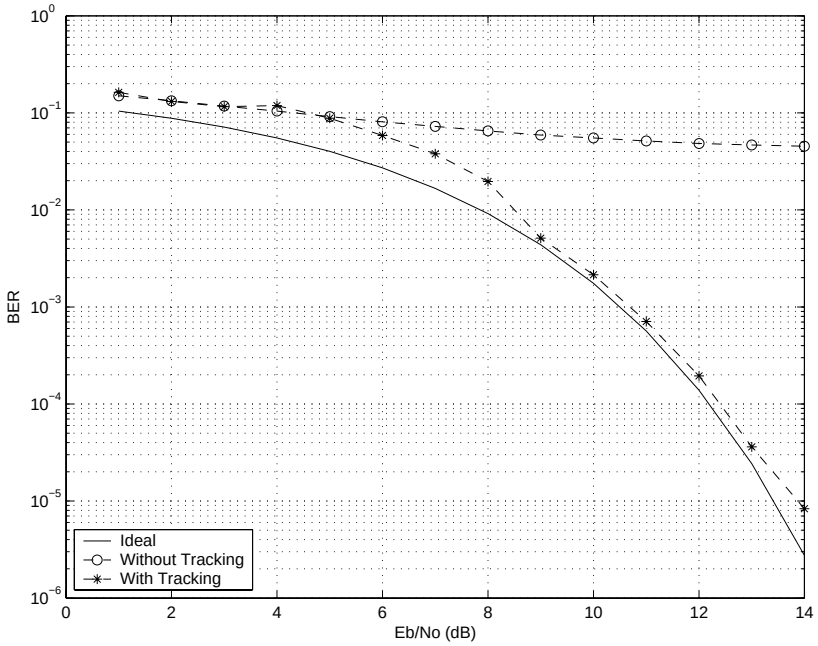

Figure 5.15 BER performance of the carrier synchronizer in the case of without and with tracking

The results in Figure 5.15 show that the BER performance with tracking is improved dramatically at moderate and large E_b/N_0 compared to the one without tracking, whereas the degradation is still significant at low E_b/N_0. This is because

the NDA phase estimation algorithm used is very sensitive to the noise level and also the function performed by the 16-th power nonlinearity is optimized for a high E_b/N_0 .

The performance of the NDA phase tracker is mainly dependent on the parameters of the frequency error Δf and the observation window size N_W . Although the bias of the estimate was removed by symmetric averaging in the algorithm for the case of $\Delta f \neq 0$, the phase tracker is still sensitive to Δf . The effect of Δf on the BER performance of the tracker at a fixed window size $N_W = 301$ symbols is shown in Figure 5.16.

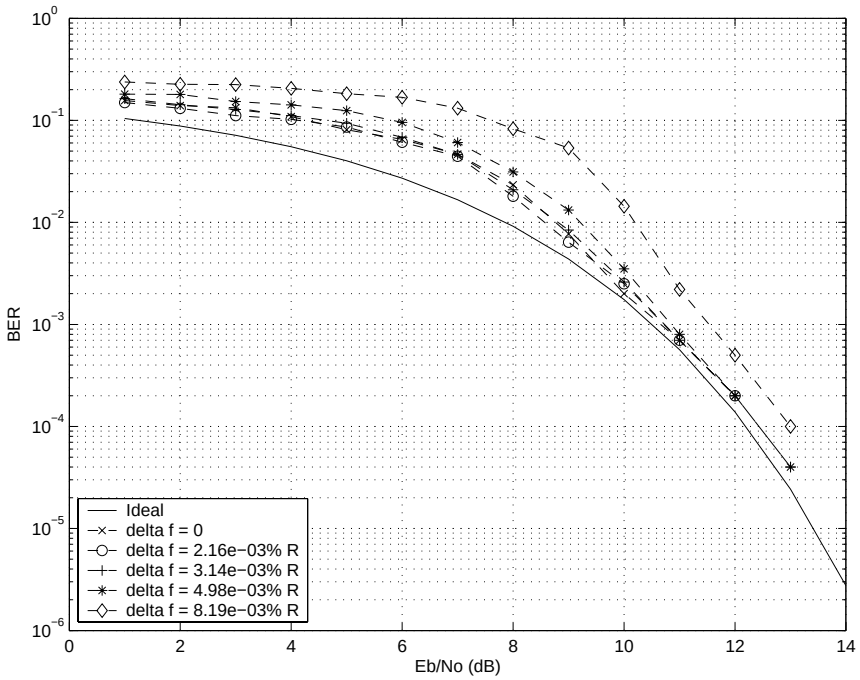

Figure 5.16 BER performance of the phase tracker for various Δf

Figure 5.16 shows that Δf yields an increase of the BER degradation as compared to $\Delta f = 0$ and the BER performance decreases with increasing Δf. In order to obtain better BER performance, it is required that the residual frequency error is a small fraction of the symbol rate.

A number of N_W are assigned in Figure 5.17 to show their effects on the BER performance of the tracker for a given $\Delta f = 3.14e-03\%R$.

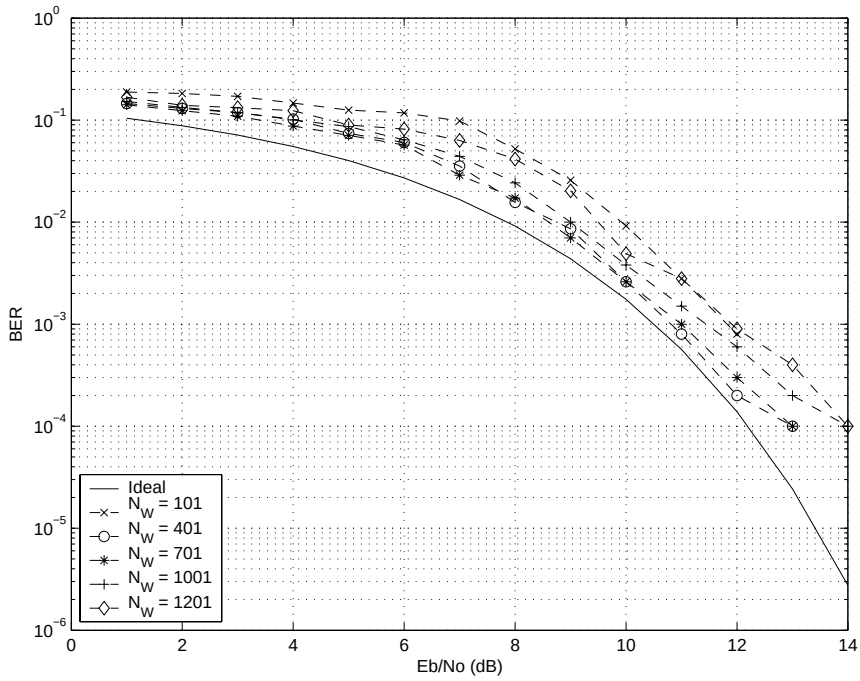

Figure 5.17 BER performance of the phase tracker for different N_W

Figure 5.17 shows that the BER performance is significantly degraded for small and large window sizes, and is optimized at some moderate window size. Clearly, an optimum value of N_W exists for $\Delta f \neq 0$. Alternatively, the observation window size can be optimized to yield minimum associated BER degradation.

5.4 Summary

The estimate bias, variance, and BER are used to evaluate and compare the estimator's performance in this chapter. Error in the estimation of synchronization parameters reduces the performance. The performance of the synchronizer can be gauged by determining the degradation in BER. In the presence of random synchronization errors, a BER degradation occurs as compared to perfect synchronization. For a small estimate variance, the BER degradation caused by random synchronization errors is essentially proportional to the estimate variance.

In this chapter, the BER performance of a DA frequency estimator, a DA phase estimator, and an NDA phase tracker were simulated and evaluated in the presence of both ideal and non-ideal conditions. DA frequency estimator accesses the estimates for 97% of the expected estimation range, and needs a longer preamble (about 101 symbols) to achieve very good performance. The frequency estimator is very sensitive to the value of the initial frequency offset because of ISI effect, and the initial frequency offset must be very small for the ISI to be neglected. DA phase estimator has proved to be unbiased for 96% of the entire range $[-\pi, \pi]$, and has the best BER performance with a short preamble (about 10 symbols). The data modulation removal process in the NDA carrier phase tracker introduces a significant amount of noise, and therefore makes the phase estimator perform badly at low SNR. The simulation has shown that even if the estimate bias caused by the residual frequency error is removed by the algorithm, the residual frequency error is still the most severe impairment for

the NDA tracker. It is very important to get more precise frequency estimation in acquisition. The observation window size in tracking can be optimized to yield minimum associated BER degradation in the presence of very small frequency error.

In all, the simulation demonstrated that the techniques provide a fast carrier acquisition (only about 111 symbols needed) and is suitable for burst-mode communication systems. The simulation also proved that this technique can be used in the IEEE 802.16 MAN system with an uncertainty of 1 ppm for a cost-effective crystal oscillator.

Chapter 6

SUMMARY, CONCLUSIONS AND RECOMMENDATIONS

6.1 Summary

The primary objective of this thesis is to develop a carrier recovery system for burst-mode 16-QAM (the symbol timing is assumed perfectly synchronized in the receiver). In burst-mode communication system, an efficient synchronization must be used. The synchronizer must synchronize itself during the relatively short burst preamble. Use of preambles reduces the transmission efficiency; therefore rapid acquiring synchronizers are needed to minimize this overhead. Some potential methods for rapid carrier synchronization have been studied and analyzed. In order to avoid hang-up and possibility of poor transient behaviour etc., it is worth using feedforward (open-loop) synchronization methods (as opposed to PLL-based methods). A feedforward DA digital carrier synchronization technique to achieve fast and reliable carrier acquisition for 16-QAM was then proposed, and the appropriate ML-based parameter estimation algorithms for carrier recovery have been derived.

The synchronization algorithms derived include the DA carrier frequency estimation and DA carrier phase estimation in acquisition, and the NDA carrier phase estimation in tracking. DA carrier frequency and phase estimation algorithms are conducted based on oversampling of a known preamble. Oversampling has advantages in that it accelerates the speed of the estimation and does not require knowledge of symbol timing. On the other hand, it places an increased computational load on the receiver. The NDA carrier phase estimation is based on the V&V phase estimation algorithm and the estimates are extracted from the random data portion of the burst packet with the aid of symbol timing knowledge. The algorithms have been tested in Matlab to verify their functionality. The BER performance of the developed estimators has been analytically evaluated and compared in the presence of some impairments (frequency offset, phase offset, and AWGN). The estimators' performance is tested under different situations, including different preamble length, different initial frequency offset, different residual frequency offset, and different observation window size.

The issue of imperfect recovery of one parameter (e.g. the inaccurate frequency estimation) on the estimation of another one (e.g. the phase estimation) also has presented. The sensibility of the proposed estimators to incorrect estimation values of those parameters has been studied to get a better view on the working of the proposed structures.

6.2 Conclusions

The carrier recovery technique presented in this thesis proved to be applicable to the modulation schemes of 16-QAM. The simulation demonstrated that the technique provide a fast carrier acquisition using a short preamble (about 111 symbols) and suitable for burst-mode communication systems.

Simulation has shown that DA frequency estimation can be done using feedforward structures with large estimation range and good performance. It operates independently of the phase offset estimation. Increasing the preamble length will improve the performance significantly. The trade-off between estimation range and estimation accuracy has been shown with respect to the correlation distance. Simulation also showed that the ISI arising from filter mismatch results in significant estimate bias and performance degradation when the initial frequency offset is large.

DA phase estimator has the best performance with a short preamble (about 10 symbols), but the estimation is dependent on the frequency offset estimation. Fortunately, due to very small residual frequency estimation error delivering from the DA frequency estimator and the very short preamble needed for the phase offset estimation, the phase variation over the phase estimation is not significant and can be ignored.

NDA phase estimator algorithm is based on the nonlinear transform to remove the data modulation. The BER performance is significantly improved for moderate and large SNR, whereas the degradation is more significant for lower SNRs. This is

because the function performed on the amplitude in the nonlinear block has been optimized for a high SNR. Simulation has also shown that even though the bias of the estimate is removed by symmetric averaging, the phase tracker is still sensitive to frequency errors. In order to obtain reasonable values of the BER degradation, it is required that the frequency error be a small fraction of the symbol rate. Alternatively, a sufficiently accurate frequency correction must be applied before the averaging over the observation window is performed, so that the residual frequency error at the input of the averaging filter does not exceed the required small fraction of the symbol rate.

In general, the frequency error is the most severe impairment for the phase estimation, especially in the tracking stage. It is required that the frequency offset estimation in acquisition should be as accurate as possible. In order to get more accurate frequency offset estimation in acquisition, the most effective way in this estimator is to increase the preamble size. We should take the range of the residual frequency offset that can be tolerated into account when choosing the preamble size. Also we should keep in mind that the preamble size should be made as small as possible to provide efficient transmission in the burst-mode scenario.

6.3 Recommendations for Future Study

This thesis does not claim, in any way, to have covered the subject in its entirety. There remain several issues that can be used as starting points and/or central themes for future studies.

Since the frequency error is most impairment for the phase tracking, also we do not want to use the way of increasing preamble length to minimize the frequency error in burst-mode operation, using closed-loop (feedback) carrier tracker can be considered as an alternative way to counteract against the effects of frequency error. Because the feedback synchronizer has a loop filter with perfect integrator, the tracking performance is not affected by the frequency error. In addition, the frequency error delivering from inaccurate DA frequency estimation would not be too large to cause “hang-up”.

The ISI due to mismatched filtering is another concerned degradation for the performance of the frequency estimator. In order to decrease ISI, it is recommended in the future work that, the roll-off factor of the matched filter be designed high so that the filter has a correspondingly narrow pulse shape, and/or the order of the matched filter be designed longer in the digital signal process (DSP) implementation solution.

REFERENCES

[1] S. Sampei, *Applications of Digital Wireless Technologies to Global Wireless Communications*, Prentice Hall Inc., Upper Saddle River, NJ, 1997.

[2] B. Sklar, *Digital Communications: Fundamentals and Applications*, Prentice Hall Inc., Englewood Cliffs, NJ, 1998.

[3] S. Haykin, *Digital Communications*, John Wiley & Sons Inc., New York, NY, 1994.

[4] H. Meyr, M. Moeneclaey and S. A. Fechtel, *Digital Communication Receivers: Synchronization, Channel Estimation, and Signal Processing*, John Wiley & Sons Inc., New York, NY, 1998.

[5] F. M. Gardner, *Phaselock Techniques*, John Wiley & Sons Inc., New York, NY, 1979.

[6] F. M. Gardner: "Hangup in phase-lock loops." *IEEE Transactions on Communications*, vol. COM-25, no. 10, pp. 1210-1214, 1977.

[7] H. Meyer, L. Popken: "Phase acquisition statistics for phase locked loops," *IEEE Transactions on Communications*, vol. COM-28, pp. 1365-1372, Aug. 1980.

[8] M. Luise and R. Reggiannini, "Carrier frequency recovery in all-digital modems for burst-mode transmissions", *IEEE Transactions on Communications*, vol. 43, no. 2/3/4, pp. 1169-1178, Feb./Mar./Apr., 1995.

[9] S. Kay, "A Fast and Accurate Single Frequency Estimator," *IEEE Trans. Acoust., Speech, Signal Processing,* vol. ASSP-37, pp. 1987-1990, Dec. 1989.

[10] N. Caouras, R. Morawski, and T. Le-Ngoc, "Fast carrier recovery for burst-mode coherent demodulation using feedforward phase and frequency estimation techniques," *Proceedings of the 1999 IEEE CCECE*, Edmonton, Alberta, Canada, pp. 79-83, May 9-12 1999.

[11] A. J. Viterbi and A.M. Viterbi, "Nonlinear estimation of PSK-modulated carrier phase with application to burst digital transmission," *IEEE Transactions on Information Theory*, vol. IT-29, no. 4, pp. 543-551, 1983.

[12] M. P. Fitz, "Equivocation in nonlinear digital carrier synchronizers," *IEEE Transactions on Communications*, vol. 39, no. 11, pp. 1672-1682, 1991.

[13] B. Paden, "A matched nonlinearity for phase estimation of a PSK-modulated carrier," *IEEE Transactions on Information Theory*, vol. IT-32, no. 3, pp. 419-422, 1986.

[14] J. G. Proakis, *Digital Communications*, McGraw-Hill Inc., New York, NY, 1995 (Third Edition).

[15] A. Bateman, *Digital Communications: Design for the real world*, Addison-Wesley Longman Limited, New York, NY, 1999.

[16] J. G. Proakis, *Digital Communications*, McGraw-Hill Inc., New York, NY, 1989 (Second Edition).

[17] D. C. Rife and R. R. Boorstyn, "Single tone parameter estimation from discrete-time observations," *IEEE Transactions on Information Theory*, vol. IT-20, pp. 591-598, Sept. 1974.

[18] S. A. Kay, *Modern Spectral Estimation: Theory and Application*, Prentice Hall Inc., Englewood Cliffs, NJ, 1988.

[19] A. Papoulis, *Probability, Random Variables, and Stochastic Processes*, McGraw-Hill Inc., New York, NY, 1984.

[20] M. C. Jeruchim, P. Balaban, and K. S. Shanmugan, *Simulation of Communication Systems*, Plenum Press, New York, NY, 1992.

APPENDIX A MATLAB MODULES FOR SIMULATION BLOCKS

This appendix contains main Matlab modules which provide the Matlab code for each simulation block.

Data Generator

```
% Define the M-ary number.
M = 16;
% There are k bits in a single M-ary QAM symbol.
k = log2(M);

% Define the symbol frequency Fd and the sampling frequency Fs.
Fd = 1;
Fs = 16;

% Give preamble symbols.
preamble = ([2 6 2 6 2 6 2 6 2 6]);

% Define the number of user data symbols.
data_len = 100;
% Generate a sequence of uniformly distributed random integers in
% range [0, M-1].
data = randint(data_len,1,M);

% Generate a burst packet.
burst = ([preamble data']);
```

16-QAM Mapper

```
% Map integers into complex symbols according to the 16-QAM
% constellation and Gray-encoded in the meantime.
burst_map = dmodce(burst,Fd,Fd,'qam',M);
```

Transmit Filter

```
% Design an FIR RRC filter.
% The roll-off factor of the RRC filter is 0.5.
```

```
rolloff = 0.5;
% The default time delay of the RRC filter is 3.
delay = 3;
% The input digital signal has frequency Fd. the sampling frequency
% for the filter is Fs.
[num den] = rcosine(Fd, Fs, 'fir/sqrt', rolloff, delay);

% Filter the signal to obtain the transmit waveforms.
[I_TxWaveform, t] = rcosflt(burst_map(:,1), Fd, Fs, 'filter', num);
[Q_TxWaveform, t] = rcosflt(burst_map(:,2), Fd, Fs, 'filter', num);

% Combine the I and Q components into a complex signal.
s_TxWaveform = I_TxWaveform + j*Q_TxWaveform;
```

AWGN Channel

```
% Generate AWGN.
% Assume the average SNR per bit EbNodB (in dB) is 10dB.
EbNodB = 10;
EbNo = 10^(EbNodB/10);

% Convert EbNo to EsNo.
EsNo = EbNo*k;

% Define the average power of 16-QAM symbols.
Es = 10;

% The noise variance.
noise_var = Es/EsNo*(1/2);
% The standard deviation of the noise.
noise_std = sqrt(noise_var);

% Model I and Q components of AWGN with zero mean and No/2 variance.
noise_I = randn(length(s_TxWaveform),1)*noise_std;
noise_Q = randn(length(s_TxWaveform),1)*noise_std;

% The baseband complex AWGN.
noise = noise_I + j*noise_Q;

% Add noise to the transmitted signal.
r_RxWaveform = s_TxWaveform + noise;
```

Receive Filter

```
% Filter the received signal.
r_FilterOutput = filter(num, den, r_RxWaveform);
```

DA Frequency Estimator

```
% Define the number of samples used for L_F and N_F.
L_F = 50*Fs;
N_F = 51*Fs;

% Calculate time average of the filter output.
r_aver = sum(r_FilterOutput(L_F+1:L_F+N_F).*conj(r_FilterOutput \\
```

```
(1:N_F)))/N_F;

% Frequency offset estimation.
Ω̂ = (atan2(imag(r_aver),real(r_aver)))/L_F;

% Phase derotation.
n = L_F+N_F+1:length(r_FilterOutput);
x = r_FilterOutput(n).*(exp(-j*Ω̂*n).');
```

DA Phase Estimator

```
% Define the number of samples used for N_P.
N_P = 10*Fs;

% Calculate time average of frequency-adjusted signal x.
x_aver = sum(x(1:N_P))/N_P;

% Phase offset estimation.
φ̂ = (atan2(imag(x_aver),real(x_aver)));

% Phase derotation.
n = N_P+1:length(x);
y = x(n)*exp(-j*φ̂);
```

NDA Phase Tracker

```
% Convert the sampling rate to the symbol rate.
y_symbols = y(Fs:Fs:length(y));

% Define the values of P, M, and N_W.
L = 16;
M = 16;
N_W = 97;

% NDA phase estimation.
% Calculate the magnitude (ρ) and the phase (Φ) of y_symbols.
ρ = abs(y_symbols(1:N_W));
Φ = atan2(imag(y_symbols(1:N_W)),real(y_symbols(1:N_W)));

% Apply a nonlinearity factor L to ρ and a multiplication factor M
% to Φ.
y_track = ρ.^L.*exp(j*M*Φ);

% Phase estimation.
Φ̂ = (1/M)*atan2(sum(imag(y_track)),sum(real(y_track)));

% Phase derotation.
z = y_track*exp(-j*Φ̂);
```

Demapper and Detector

```
data_recov = ddemodce(z,Fd,Fd,'qam',M);
```

BER Counter

```
[BER_NUM BER_RATIO] = biterr(data,data_recov,k);
```